Materials Today Bio 38 (2026) 103040

Contents lists available at ScienceDirect

Materials Today Bio

journal homepage: www.journals.elsevier.com/materials-today-bio

Thermoreversible cell-derived extracellular matrix only hydrogel (CEOgel): Development, characterization, and applications

Byoungha An [a,b], Jae Won Kwon [a], Heejeong Yoon [c], Tae-Eun Park [c], Seung Won Yang [a,b], Kwideok Park [a,b,*]

[a] Center for Biomaterials, Korea Institute of Science and Technology (KIST), Seoul, 02792, Republic of Korea
[b] Division of Bio-Medical Science and Technology, KIST School, University of Science and Technology (UST), Seoul, 02792, Republic of Korea
[c] Department of Biomedical Engineering College of Information and Biotechnology Ulsan National Institute of Science and Technology (UNIST), Ulsan, 44919, Republic of Korea

ARTICLE INFO

Keywords:
Cell-derived extracellular matrix
Decellularized extracellular matrix
ECM hydrogel
Thermosensitive
Thermoreversible

ABSTRACT

Decellularized extracellular matrix (dECM) has been widely used as a biomimetic material for three-dimensional cell culture and tissue regeneration. Although tissue-derived ECM is the conventional source of dECM, cell-derived ECM (cECM) has emerged as an attractive alternative. Various cECM-based formulations such as powders, films, and preformed gels have been reported, but thermosensitive cECM hydrogels remain largely unexplored.

Here, we report a novel method to produce a thermoreversible hydrogel exclusively made from cECM, termed CEOgel. Once *in vitro*–cultured umbilical cord mesenchymal stem cells were decellularized, cECM solubility was enhanced and its nanofibers were concentrated to generate CEOgel without additional factors. This fabrication strategy was applicable across multiple cell types and consistently yielded homogeneous gels with minimal donor- or batch-dependent variability. CEOgel exhibited sufficient mechanical stability for *in vitro* use and formed gels *in vivo* following injection, confirming its thermosensitive and biocompatible nature. It also served as a functional 3D matrix, supporting endothelial vascularization in microfluidic chips and the growth of colorectal cancer organoids. Proteomic profiling revealed that CEOgel incorporates a broad spectrum of proteins commonly expressed across human tissues. Additionally, we demonstrated that CEOgel properties can be tuned through transition-metal crosslinking and genetically engineering ECM-producing cells.

Together, this study proposes a new class of thermoreversible cECM hydrogels that eliminate reliance on animal tissues or external cross-linkers while expanding the applicability of cECM materials and advancing conceptual diversity for ECM hydrogel design. Our findings highlight the potential of CEOgel as a regenerative biomaterial for tissue engineering and medical applications.

1. Introduction

The extracellular matrix (ECM) is a complex and dynamic network of macromolecules secreted by various cell types. As the non-cellular component of all tissues, the ECM provides tissue-specific microenvironments that not only offer structural support but also regulate essential cellular processes, such as cell survival, differentiation, and homeostasis through physical and biochemical cues. Consequently, extensive efforts have been made to develop biomaterials that recapitulate the architecture and composition of native ECM to guide complex, sequential cellular behaviors relevant to tissue regeneration [1]. However, ECM-derived natural polymers such as collagen, hyaluronic acid, and gelatin remain too simplistic to captur e the structural and biochemical complexity of native ECM, which comprises diverse proteins, proteoglycans, and glycosaminoglycans (GAGs) and bioactive factors [2].

Accordingly, decellularized tissue–derived extracellular matrix (tECM) has gained significant attention as a biomimetic biomaterial that closely preserves the composition and architecture of native ECM. Clinically, several tECM-based products have been approved by the U.S. Food and Drug Administration (FDA) for applications such as soft tissue repair [3]. In research, tECM-based hydrogels (tECMgel) have been

* Corresponding author. Center for Biomaterials, Korea Institute of Science and Technology (KIST), Seoul, 02792, Republic of Korea.
E-mail address: kpark@kist.re.kr (K. Park).

https://doi.org/10.1016/j.mtbio.2026.103040
Received 7 January 2026; Received in revised form 25 February 2026; Accepted 17 March 2026
Available online 17 March 2026

widely adopted for three-dimensional (3D) cell culture, providing tissue-specific microenvironments. However, tECM also faces inherent challenges, including the limited availability of donor tissues—particularly cadaveric sources—and technical difficulties in isolating certain ECM types, such as those from small or inaccessible tissues (e.g., stem cell niches). Moreover, risks of immunological rejection and disease transmission remain [4]. And the fixed compositions of tECM makes it difficult to tailor its biochemical or mechanical properties for specific experimental or clinical purposes [5].

In this context, cell-derived ECM (cECM) has emerged as a promising alternative because it retains the biochemical complexity of native ECM while addressing several limitations of tECM [6]. Since cECM is produced in a controlled *in vitro* culture environment, it is more accessible and exhibits reduced batch variability, immunogenicity, and risk of disease transmission [7].Moreover, the decellularization process for cECM is typically shorter and milder than that for tECM, helping to preserve more bioactive molecules [8]. In particular, cECM offers greater flexibility for customization by selecting the ECM-producing cell type or by modulating cellular behavior through genetic or culture-condition changes. Unlike tECM, which represents the bulk composition of an entire tissue, cECM can provide cell-type-specific microenvironments. Owing to these advantages, research on cECM-based biomaterials has expanded rapidly in recent years. For instance, alginate hydrogels incorporating cECM have been shown to accelerate skin wound healing by retaining mesenchymal stem cell (MSC) secretomes [9]. MSC spheroid-derived decellularized ECM has been reported to mitigate traumatic brain injury [10], and stretchable fibroblast-derived ECM patches have been developed to enhance stem-cell delivery for cardiovascular repair [11].

However, few reports have described thermosensitive hydrogels made solely from cECM. Fibroblast-derived cECM hydrogel have been shown to promote skin wound remodeling but cannot undergo sol-gel transition, existing only as pre-formed gels [12]. Injectable hydrogel based on BMSC-derived cECM has been developed for cartilage regeneration, yet this required more than 30% agarose to achieve gelation [13]. Similarly, human fibroblast-derived matrix composite hydrogel prepared by conventional tECM hydrogel methods failed to form stable gels unless combined with cross-linkers or other polymers such as fibrin or collagen [14]. In contrast, more than 70 studies have reported thermosensitive hydrogels derived from animal or cadaveric tissues across multiple organs [15], whereas successful examples prepared solely from cECM remain scarce. The absence of an intrinsic thermoresponsive sol–gel transition near physiological temperature limits the application of cECM-based materials as injectable systems and 3D cell-encapsulating matrices. In many cases, cECM has been used primarily as a coating material in 2D systems, while suspension, sheet, or pre-formed gel formats restrict minimally invasive transplantation by injection Moreover, blending cECM with additional polymers or cross-linkers may dilute its unique advantage of providing cell-type–specific extracellular environments. Therefore, developing a thermosensitive hydrogel composed exclusively of cECM may enable the integration of the biological precision of cell-derived matrices with the versatility of phase-transitional hydrogels. Such a system could facilitate advanced 3D culture platforms and minimally invasive therapeutic delivery. Accordingly, this study aimed to fabricate a purely cell-derived, thermoresponsive ECM hydrogel.

Here, we established a novel method to fabricate a thermosensitive hydrogel composed of cECM alone. This approach is not limited to a specific cell source. The cell derived ECM-only hydrogels (CEOgels) were successfully generated from the ECM produced by umbilical cord mesenchymal stem cells (UCMSCs), skin fibroblasts, and genetically modified HEK293T cells. The resulting CEOgel exhibited sufficient mechanical stability for both *in vitro* and *in vivo* applications and displayed thermo-reversible behavior, forming a gel at 37 °C and reverting to a sol state upon cooling. We characterized the CEOgel fabrication process and gelation mechanism and investigated its biochemical, mechanical, and microarchitectural properties. Proteomic analysis revealed the molecular composition of CEOgel and confirmed the reproducibility of the fabrication process across batches and donors, as well as the similarity of its protein profile to those of various human tissues. We further demonstrated strategies to modulate the physical properties and biochemical composition of CEOgel through cross-linking and genetic engineering of ECM-producing cells. Finally, the biocompatibility and *in vivo* safety of CEOgel were verified, and its suitability as both a 3D cell-culture matrix and an injectable hydrogel was established.

2. Results and discussion

2.1. CEOgel fabrication and its gelation mechanisms

2.1.1. CEOgel was fabricated using novel strategies designed to enhance cECM solubility

To fabricate CEOgel, we employed a specialized process distinct from conventional approaches used to generate tissue-derived ECM hydrogels. Animal-derived ECM hydrogels typically undergo gelation through collagen-driven self-assembly. However, applying the same procedure to cell-derived ECM failed to form gels or produced hydrogels that were too unstable to withstand standard laboratory handling [14], likely due to compositional differences between tissue-derived and cell-derived ECM. To overcome this limitation, we developed fabrication strategies aimed at enhancing the solubility of cECM, thereby increasing the proportion of the components available for polymerization in the condensed sol state.

Initially, the cECM obtained from decellularization of cultured cells (Fig. 1A–1) was processed into powder form (Fig. 1A–2,3) and subjected to enzymatic digestion (Fig. 1B–4). Next, for the first strategy, the enzyme-digested cECM was neutralized (Fig. 1B–5) prior to freeze-drying to obtain enzyme-digested cECM powder (Fig. 1B–6). As shown in Fig. 2A, neutralization markedly increased the transmittance of the digested solution, which indicates enhanced solubility of cECM components under neutral conditions. Importantly, this enhanced solubility also exerted a prolonged effect during the subsequent reconstitution of the enzyme-digested cECM, enabling improved solubilization of ECM components and the preparation of condensed cENF solution (Fig. 1C–7). Notably, neutralization prior to freeze-drying was essential, as neutralization performed after reconstitution failed to produce thermoresponsive gelation (data not shown).

As the second strategy, sonication followed by incubation at 4 °C was applied during reconstitution of the enzyme-digested cECM powder. This approach was adapted from a protocol for preparing collagen nanofiber solutions, in which collagen fibers are reduced to the nanometer scale and form hydrogels at 37 °C with properties distinct from conventional collagen gels [16]. Consistent with this rationale, the cECM fiber size was significantly reduced, and more uniform nanometer-scale population was obtained in the cENF solution, as confirmed by DLS analysis (Fig. 2B). This improvement in homogeneity enabled the preparation of a uniformly dissolved and condensed cENF solution, at the comparatively high concentration of 67 mg/mL (Fig. 1C–7). Collectively, this step increases both the effective ECM concentration and fiber number density, creating conditions favorable for thermoresponsive gelation. While these processing strategies enable thermoresponsive gelation of CEOgel, the precise molecular and physical mechanisms underlying this behavior remain to be fully elucidated and will be the focus of future studies.

2.1.2. CEOgel demonstrates thermoreversibility, revealing distinctive gelation mechanisms

Then, the optimized processes, along with the key gelation characteristics, were subsequently examined to clarify the mechanism and properties of CEOgel. The cENF solution prepared using our strategies underwent sol–gel transition at 37 °C to form CEOgel (Fig. 1C–8). Because there was no significant difference in total mass between cECM

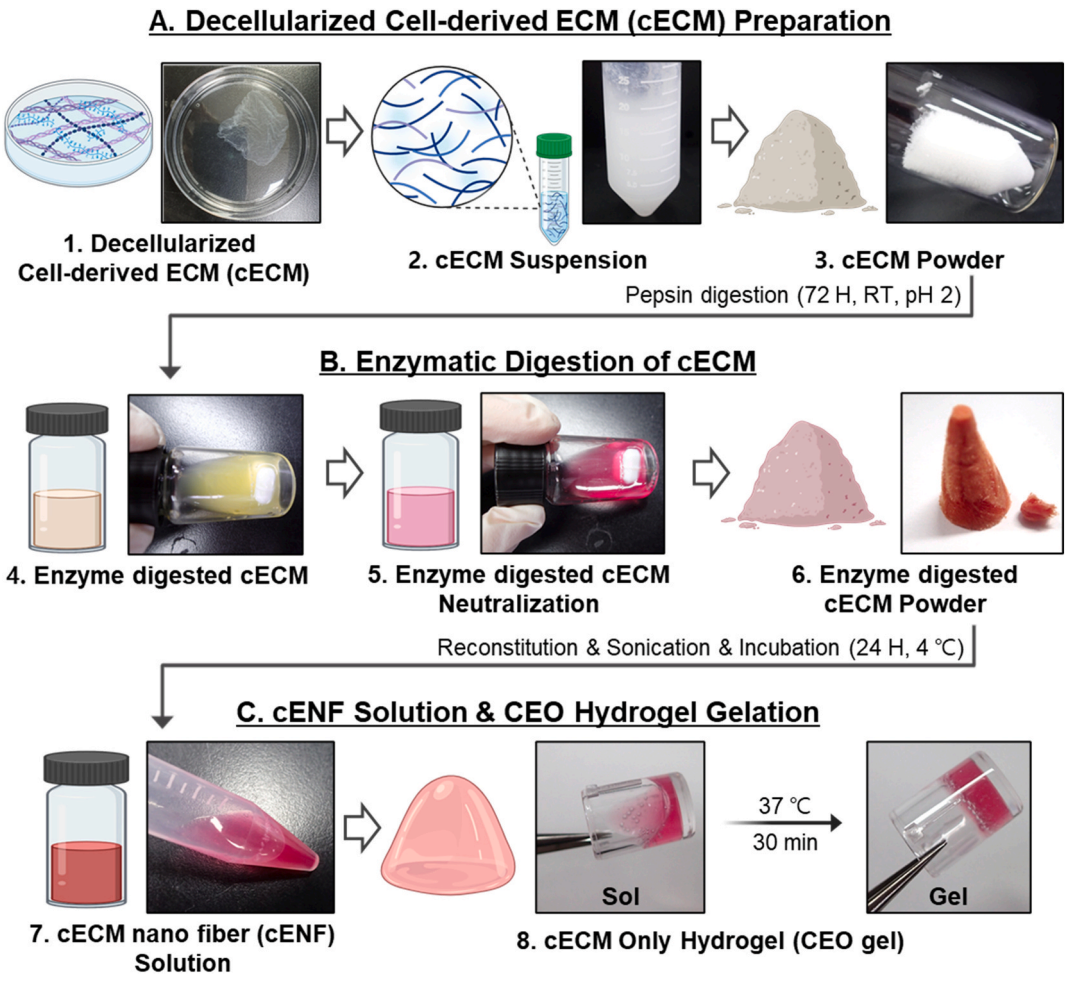

Fig. 1. Preparation of CEOgel. **(A)** ECM was obtained by decellularizing cultured cells, followed by sonication and freeze-drying to produce cECM powder. **(B)** The cECM powder was enzymatically digested with pepsin and lyophilized to generate enzyme-digested cECM powder. **(C)** The cENF solution was prepared by reconstituting the concentrated enzyme-digested cECM powder, and CEOgel was formed by incubating the cENF solution at 37 °C for 30 min. The figure was created with BioRender.

and the final enzyme-digested cECM powder (Fig. S1A), we assume that CEOgel provides an environment closely resembling the native cECM where the cells originally resided. Furthermore, this fabrication method was not restricted to a specific cell type, as demonstrated by successful gel formation with cECM derived from different cell sources, including skin fibroblasts (Fig. S2). Unless otherwise noted, subsequent analyses were performed using UCMSC-derived CEOgel as a representative model.

As CEOgel becomes opaque during polymerization, turbidity was monitored to assess gelation kinetics. Both 67 mg/mL and 33 mg/mL CEOgel displayed sigmoidal gelation curves with comparable kinetic parameters, including gelation rate (S), half-gelation time ($t_{1/2}$), and lag time (t_{lag}) (Fig. 2C). Notably, CEOgel reached 90% gelation within 30 min, with a $t_1/_2$ (≈14 min) and t_{lag} (≥9.5 min) that were on the faster side relative to previously reported values for tissue-derived ECM hydrogels (Fig. 2D) [17–19].

To further evaluate the concentration-dependent gelation properties, tube inversion assays were performed with cENF solutions of varying concentrations. At 10 mg/mL, the sol flowed freely upon inversion, while the 20 mg/mL sol required ~1 h of incubation at 4 °C before flowing. In contrast, higher concentrations (>20 mg/mL) showed no flow even after prolonged incubation at 4 °C. Following 1 h incubation at 37 °C, all samples except the 10 mg/mL group formed stable gels in inverted tubes (Fig. 2E). These results indicate that increasing sol concentration enhances viscosity, and that a minimum of 10 mg/mL is required for stable gel formation.

Interestingly, CEOgel displayed thermoreversible behavior over four warming–cooling cycles, although repeated cycling gradually weakened gel forming capability (Fig. 2F). This property is distinct from conventional collagen gels and has been rarely reported in tissue-derived ECM hydrogels, which are primarily based on collagen fibrillogenesis [15, 20]. These findings suggest that the gelation mechanism of CEOgel is not governed solely by collagen-driven assembly but instead involves features of physically crosslinked thermoreversible hydrogels.

Next, to investigate the gelation mechanism, we examined the major interactions within the formed CEOgel using dissociation assays, as previously reported [21]. CEOgels were incubated in different dissociation reagents: SDS to disrupt hydrophobic interactions, urea to disrupt hydrogen bonds, and 2-ME to reduce disulfide bonds. Gel dissociation was quantified by measuring residual gel size (Fig. 2G). Notably, CEOgel exposed to 0.6 M urea was rapidly degraded, with the entire structure disappearing within 15 min. SDS also destabilized the gel, leading to complete dissociation within 60 min, whereas 2-ME did not appreciably alter the gel structure compared with the distilled water control. These results indicate that hydrogen bonding plays the dominant role in the formation of the CEOgel network, with hydrophobic interactions contributing to a lesser extent.

As about 50% of CEOgel is composed of proteins (Fig. S1B), we next examined their molecular weight distribution using SDS–PAGE. The results revealed a wide size range, from <25 kDa to >300 kDa (Fig. 2H).

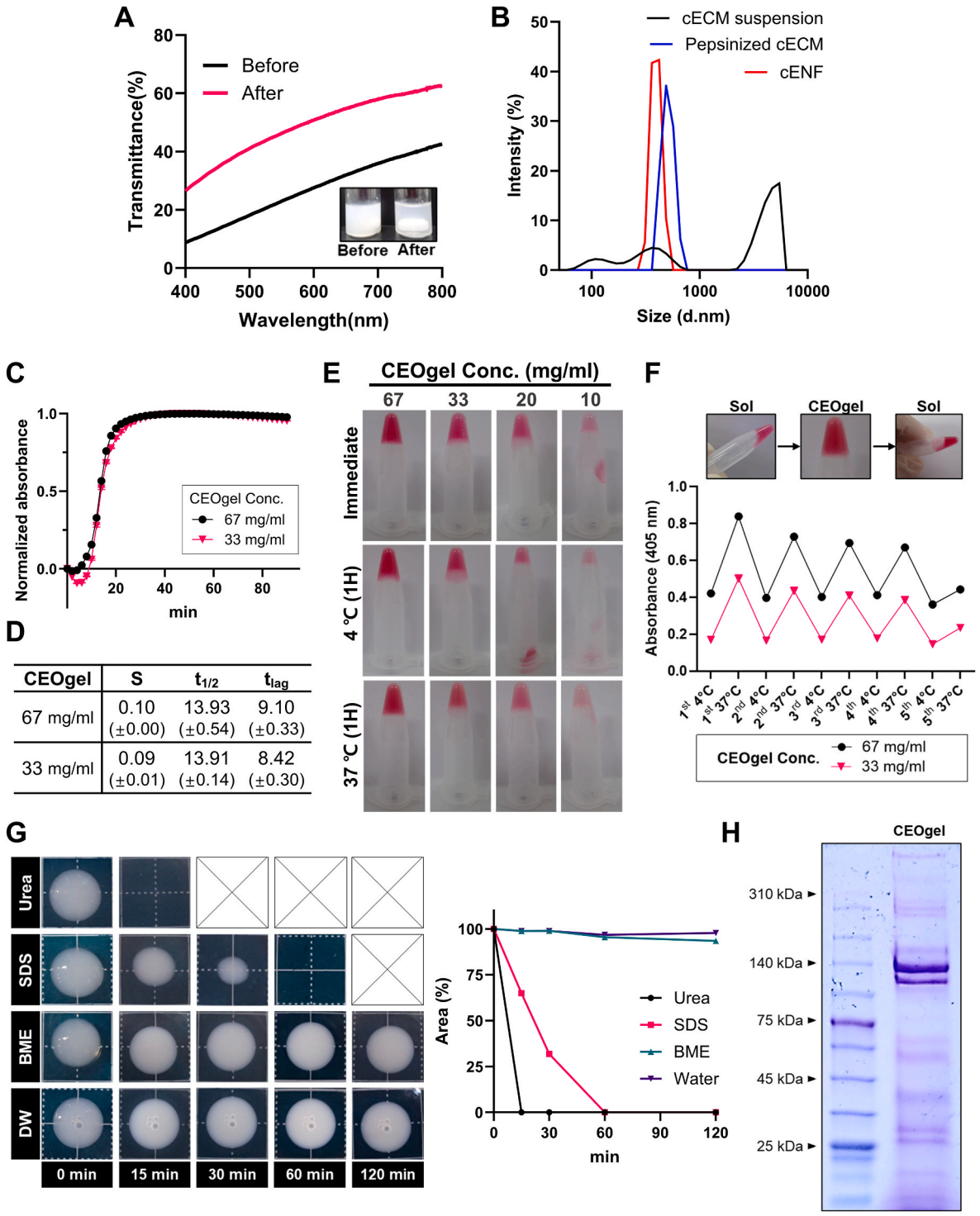

CEOgel	S	$t_{1/2}$	t_{lag}
67 mg/ml	0.10 (±0.00)	13.93 (±0.54)	9.10 (±0.33)
33 mg/ml	0.09 (±0.01)	13.91 (±0.14)	8.42 (±0.30)

Fig. 2. The Gelation mechanisms of CEOgel. **(A)** Light transmittance was quantified over the visible spectrum of light before and after neutralizing enzyme-digested cECM. **(B)** Size distributions of cECM suspension, pepsinized cECM and cENF solution were measured by dynamic light scattering. **(C)** Absorbance at 405 nm was measured during five successive cooling (4 °C) and warming (37 °C) cycles to evaluate the repeated sol–gel transitions. Two different concentrations of cENF solution (33 mg/mL and 67 mg/mL) were tested. **(D)** Turbidimetric gelation kinetics of CEOgel were analyzed using cENF solutions at 33 and 67 mg/mL by measuring absorbance at 405 nm at 2 min intervals (n = 3). Absorbance data were normalized by setting the initial and maximum readings to 0 and 1, respectively. **(E)** Gelation kinetic parameters were calculated from turbidimetric analysis of CEOgel formation at concentrations of 33 and 67 mg/mL over 90 min (n = 3). t_{lag}: lag phase; $t_{1/2}$: time to reach half of the maximum turbidity; *S*: gelation rate. **(F)** Photographs of CEOgel at various concentrations were taken immediately after tube inversion, after 1 h incubation at 4 °C and at 37 °C, respectively. **(G)** Electrophoretic profiles of CEOgel were analyzed by SDS–PAGE followed by Coomassie Brilliant Blue staining. **(H)** Photograph images of CEOgel (67 mg/ml) were taken after soaking in various dissociation regents for 2 h. The remaining CEOgel area at each time point was quantified using ImageJ. (For interpretation of the references to color in this figure legend, the reader is referred to the Web version of this article.)

Although we did not further analyze the specific roles of these proteins in CEOgel polymerization, it will be important to identify which components play a dominant role in physical crosslinking. Considering the abundance of high–molecular-weight proteins and the thermoreversible property of CEOgel, it is also worthwhile to investigate whether topological entanglement contributes to gel formation.

Taken together, we successfully developed a new method to fabricate CEOgel from cECM without the need for additional cross-linkers or gelation-inducing components. Physical interactions, particularly hydrogen bonding, appear to be the primary contributors to gelation, with viscosity and polymerization dependent on sol concentration. Moreover, CEOgel exhibits thermoreversible behavior and shows gelation kinetics comparable to those of tissue-derived ECM hydrogels.

2.2. The characterization of CEOgel

2.2.1. Analysis of biochemical composition and ECM constituents of CEOgel

Next, we carried out a detailed characterization of CEOgel. To assess the efficiency of the decellularization process, we quantified residual DNA before and after the process. Approximately 99.3% of DNA was removed, leaving 47.37 ng dsDNA per mg dry ECM (Fig. 3A), which not only demonstrates high decellularization efficiency but also indicates a reduced risk of immunogenicity, as this value falls below the generally accepted threshold of 50 ng dsDNA per mg ECM [22]. Additionally, the concentrations of total protein and glycosaminoglycans (GAGs)—the major ECM components—were 31.07 mg/mL, accounting for slightly less than half of the total mass (Fig. S1B), and 4.7 mg/mL, respectively (Fig. 3B). These results indicate that more than 90 % of the proteins and GAGs present in the original cECM are preserved after CEOgel fabrication (Fig. S3A and B).

Moreover, CEOgel was found to contain various bioactive factors, as determined using a growth factor antibody array (Fig. 3C). Through the quantification of chemiluminescence intensity, we ranked the growth factors which showed at least 40 % intensity of positive control. According to the functional annotation results from the analysis using DAVID [23,24] most of the growth factors were associated with positive regulation of cell population proliferation (GO:0008284). And notably, angiogenesis (GO:0001525) related growth factors, such as PDGFA, VEGFD, EGF, PDGFB, are highly ranked (Supplementary Data).

The representative cECM proteins—collagen type I (COL I), fibronectin (FN), and laminin—were also examined by western blot and immunofluorescence (IF). Western blot analysis showed that COL I, FN, and laminin were present both before and after decellularization, whereas GAPDH, an intracellular protein, was absent in cECM, confirming efficient removal of cellular components. (Fig. 3D). IF staining further revealed that COL I, FN, and laminin were evenly distributed in a net-like pattern within CEOgel (Fig. 3E). Using FN as a reference [9], quantification confirmed higher levels of COL I and FN compared with laminin, and no DAPI signal was detected, indicating the absence of residual DNA.

2.2.2. Analysis of microstructural and physicochemical properties of CEOgel

To investigate the microstructure of CEOgel, scanning electron microscopy (SEM) was performed on gels prepared at 67 and 33 mg/mL, respectively. SEM images revealed a porous architecture formed by interwoven nanofibers distributed throughout the matrix (Fig. 3F). At higher concentration, the fibrous network appeared denser and more compact. In addition, protein staining of cross-sections using Coomassie blue showed that proteins were evenly distributed, forming an interconnected, net-like ultrastructure (Fig. 3G).

Rheological characteristics of CEOgel were assessed at 67 and 33 mg/mL using oscillatory frequency sweep tests at 37 °C. In both cases, CEOgel exhibited gel-like behavior, with the storage modulus (G') exceeding the loss modulus (G''), and the higher concentration gel displayed a greater G' value (Fig. 3H). The tan δ (G''/G') of both gels was <1, confirming solid-like properties, and was lower in the 67 mg/mL gel. These results indicate that CEOgel forms a gel-like network at both concentrations, with increased concentration enhancing solid-like behavior (Fig. 3I). Comparative analysis showed that the G' value of CEOgel at 67 mg/mL was comparable to that of Matrigel and higher than that of liver-derived tECMgel (Fig. S3D–F), indicating similar elastic stiffness between CEOgel and Matrigel, and greater stiffness relative to tECMgel at this concentration. Furthermore, at the lower concentration of 33 mg/mL, the elastic modulus (G') of CEOgel was lower than that of tECMgel. These findings indicate that the elastic properties of CEOgel can be modulated by concentration, allowing its stiffness to be tuned within the range of commonly used ECM hydrogels.

In addition, the biodegradability of CEOgel was evaluated *in vitro* for 7 days using collagenase and dispase. Protein release from the gels was quantified at each time point. Approximately 50% of the proteins were released within 8 h for both 33 and 67 mg/mL gels, while more than 80% was released by day 7 (Fig. 3J), which is comparable to the degradation rate observed for the same volume of Matrigel and tECMgel (Fig. S3C). Notably, the release profiles were nearly identical between the two concentrations, suggesting that degradation is largely concentration-independent. This may be explained by the fact that CEOgel polymerization is not driven solely by proteins such as collagen; thus, the presence of protein-degrading enzymes did not result in markedly different degradation rates between the two groups.

The transparency of CEOgel was also evaluated, as optical clarity is an important property for biomaterials that require microscopic observation, such as 3D cell culture matrices. According to the results all three concentrations of CEOgel (67, 33, 20 mg/mL) permitted light transmission (Fig. 3K). Quantitatively, although transmittance decreased with increasing concentration, all samples exhibited at least 50% transmittance at the end of the visible spectrum. Notably, the 20 mg/mL CEOgel showed $>80\%$ transmittance. These findings confirm that CEOgel possesses sufficient transparency for observation under bright-field microscopy.

Following characterization, we explored an optional proof-of-concept strategy to further modulate the physical properties of CEOgel. Based on previous reports showing that $K_2Pt(II)Cl_4$ enhances the stiffness and transparency of collagen nanofiber hydrogels [16], transition metal complexation was applied to CEOgel. Incorporation of $K_2Pt(II)Cl_4$ significantly increased both stiffness and optical transmittance of CEOgel (Fig. S4). Although CEOgel inherently forms a hydrogel without external cross-linkers, these results demonstrate the feasibility of additional physical modulation when required.

Based on the comprehensive analysis, we confirmed the decellularization efficiency of CEOgel and identified both representative ECM proteins and bioactive growth factors. In addition, we evaluated its physical, microstructural, biodegradable, and optical properties, providing baseline information that supports the use of CEOgel in diverse applications, ranging from 3D cell culture matrices to regenerative biomaterials.

2.3. Proteomic profiling of CEOgel

2.3.1. cECM exhibits minimal donor and batch variability

Next, we performed extensive proteomic analysis of cECM using mass spectrometry to investigate protein compositions after decellularization. Compared with tissue-derived ECM, proteomic information on cell-derived ECM is limited, and specifically, reports on UCMSC-derived cECM are scarce. Because UCMSCs are primary cells, it is also important to validate whether donor and batch variability influence ECM composition, as consistency of cECM components is essential to ensure the reproducibility in CEOgel production. Therefore, we not only profiled the proteomic components of cECM from multiple perspectives but also assessed donor and batch effects on protein composition.

More than 3400 proteins were identified in UCMSC-derived cECM,

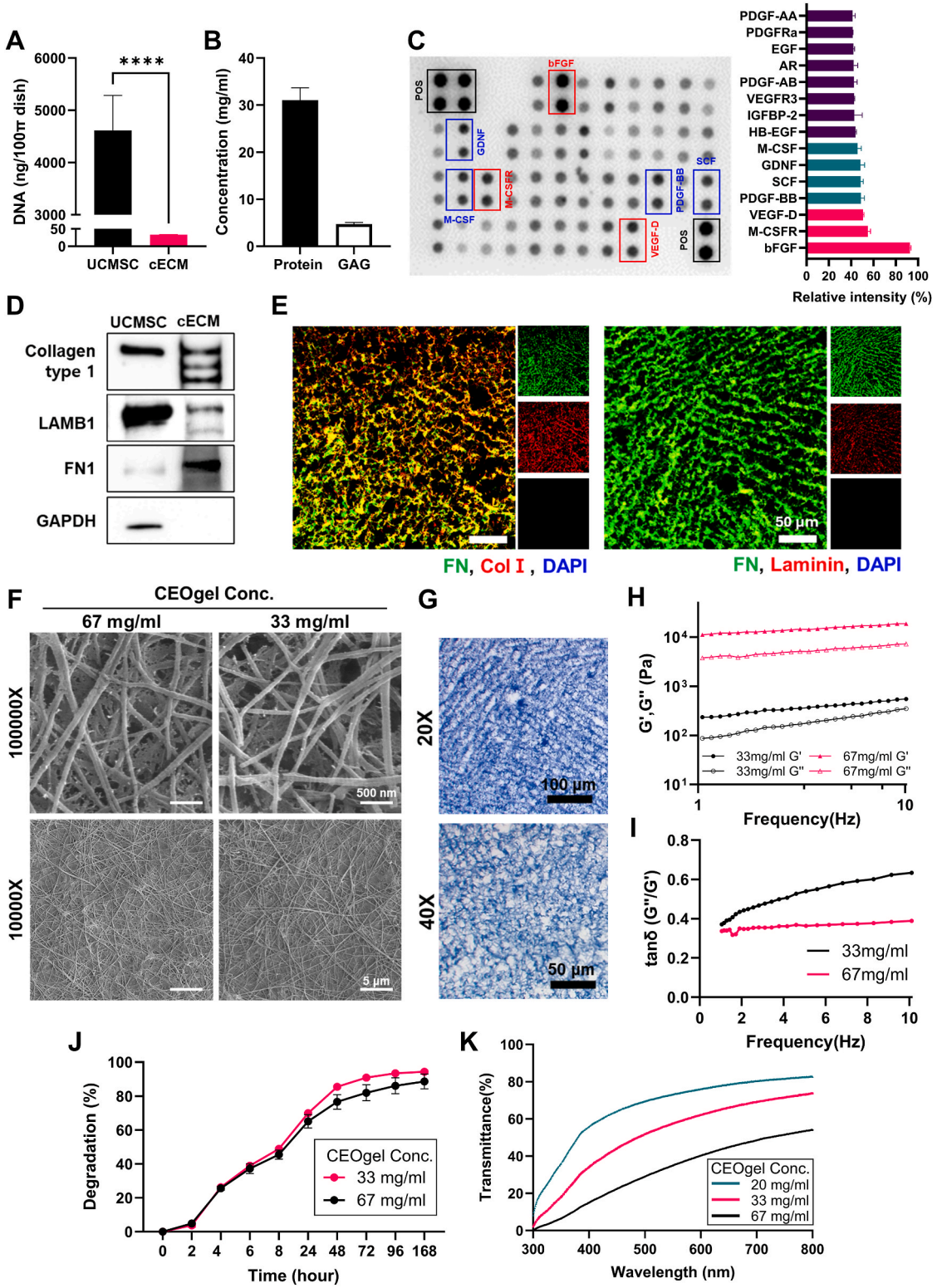

Fig. 3. The Characterization of CEOgel. **(A)** Residual DNA content was quantified before and after decellularization (n = 6). **(B)** Protein and glycosaminoglycan (GAG) contents were quantified (n = 3). **(C)** Image of human growth factor antibody array membrane. Relative signal intensities of each spot were normalized to the positive control, and the top 15 growth factors are presented in the graph. **(D)** The representative ECM proteins (collagen type 1, laminin and fibronectin) were detected by western blot before (UCMSC) and after decellularization (cECM). **(E)** Immunofluorescence staining of representative ECM proteins in CEOgel (blue: DAPI, green: fibronectin, red: collagen type I, laminin; scale bars = 50 μm). **(F)** Scanning electron microscopic (SEM) images display the internal microstructure of CEOgel. (scale bars for 100,000X: 500 nm; for 10,000X: 5 μm) **(G)** Total protein distribution was visualized by coomassie brilliant staining (scale bars for 20X: 100 μm; for 40 X: 50 μm) **(H)** Rheological profile of CEOgel at 33 and 67 mg/mL were obtained from oscillatory frequency sweep tests at 37 °C showing storage modulus (G′), loss modulus (G″) and **(I)** tanδ. **(J)** Biodegradation rates of CEOgel (33 and 67 mg/mL) were assessed over 7 days in the presence of collagenase and dispase. **(K)** Light transmittance across the visible spectrum was measured for CEOgel at three concentrations (20, 33 and 67 mg/ml). Data are presented as mean ± SD; ****$p < 0.0001$. (For interpretation of the references to color in this figure legend, the reader is referred to the Web version of this article.)

including up to 203 matrisome proteins filtered using MatrisomeDB$^{2.0}$ [25]. To evaluate variations, we compared matrisome protein diversity under two conditions: (1) batch variation, defined as cECM derived from the same donor but different cell batches cultured at different time points (e.g., Donor A1 vs. A2); and (2) donor variation, defined as cECM derived from different donors (Donor A vs. Donor B). Remarkably, the matrisome profiles were highly similar across both batch and donor comparisons (Fig. 4A), with 183 matrisome proteins overlapping between donors and batches (Fig. 4B). Pearson's correlation coefficients and Uniform Manifold Approximation and Projection (UMAP) analysis further confirmed that cECM samples from different batches or donors displayed high similarity in their proteomic profiles (Fig. 4C and D). Collectively, these results indicate that UCMSC-derived cECM exhibits low batch-to-batch and donor-to-donor variability.

2.3.2. GO enrichment analysis reveals functional signatures of cECM, and proteomic profiling identifies key matrisome proteins

Gene Ontology Biological Process (GOBP) analysis revealed that matrisome proteins were mainly enriched in terms related to ECM organization and ECM component assembly. Interestingly, vasculature-related terms were also highly ranked, suggesting the potential of CEOgel for vascular applications (Fig. 4E). Among the top 15 representative terms from Gene Ontology Cellular Component (GOCC) analysis, most were associated with extracellular regions, as expected (Fig. 4F). Notably, vesicle- and exosome-related terms were also enriched, supporting the multifaceted role of ECM as both a structural scaffold and a reservoir of adsorbed soluble factors required for intercellular signaling [26]. Additionally, the top 10 proteins within each matrisome category were identified (Fig. 4G), providing representative profiles of the major ECM components present in cECM.

Interestingly, GOBP analysis of non-matrisome proteins showed that most of the top enriched terms were related to translation, ribosome, and biosynthesis (Fig. S5A). Similarly, GOCC analysis revealed enrichment in ribosome-related terms, along with additional terms linked to cell adhesion, anchoring, and extracellular vesicles (Fig. S5B). These enrichment patterns resemble those previously reported for Matrigel. However, the overall proportion of non-matrisome proteins in CEOgel was comparable to that of tissue-derived ECM, with ~12% of the total proteins classified as matrisome (Fig. S5C) [27]. Taken together, these results suggest that cECM shares certain features with both Matrigel and tissue-derived ECM, yet ultimately provides a distinct microenvironment of its own.

2.3.3. cECM retains widely expressed proteins found across multiple human tissues

We examined the similarity of cECM proteomic profiles to those of human tissues. ECM hydrogels are widely recognized as suitable for 3D culture and hold strong potential in regenerative medicine because they provide environments resembling native extracellular matrices [8]. In particular, tissue-derived ECM hydrogels have been shown to exhibit proteomic profiles similar to the tissues from which they originate [26,27]. By contrast, whether cECM can mimic tissue-like environments from a proteomic perspective has been largely unanswered.

To address this, we selected the top 500 total proteins and the top 50 matrisome proteins from cECM and compared them with tissue-specific proteomic datasets [28], in which protein abundance was ranked from 1 (lowest) to 5 (highest), with absent proteins scored as 0. The results showed that most of the top 500 cECM proteins were highly expressed across 31 tissues, with the umbilical artery as an exception (Fig. 4H). Similar trends were observed in an independent dataset of 44 tissues [29], where cECM proteins again showed broad overlap, though relative similarity appeared clearer as tissues were more finely subdivided. For example, cECM proteins aligned more strongly with placenta than with smooth muscle (Fig. S5D). This tendency was also observed for the top 50 matrisome proteins, most of which showed high abundance across diverse tissues (Fig. 4I). Together, these results suggest that cECM captures many universal proteins found across diverse tissues, supporting its broad applicability. In the light of these findings, further analysis to identify tissue-specific proteins in cECM could help guide more tailored applications.

From the proteomic analysis, we confirmed that our preparation method yields cECM of homogeneous quality in terms of proteomic profiles. The top matrisome proteins within each category were identified, and enrichment analysis of GOBP and GOCC terms highlighted their functional associations. Finally, by demonstrating that cECM conserves many universally expressed proteins across human tissues, we established its potential for a wide range of applications. Further investigation into tissue-specific signatures, combined with proteomic analysis of cECMs derived from diverse cell types, will help refine its use in more targeted contexts.

2.4. CEOgel composition can be customized through genetic engineering of ECM-producing cells

In general, natural polymer–based hydrogels have limited control over composition and tunability. As a proof-of-concept strategy to overcome this limitation, we explored the fabrication of CEOgel from genetically modified cells. Unlike conventional natural polymers, cell-derived ECM offers a clear advantage, as its composition can be customized by genetically engineering the ECM-producing cells using well-established methods [30]. To demonstrate this concept, we employed a COL1A1-overexpressing cell line to generate type I collagen–enriched cECM for CEOgel fabrication (Fig. 5A).

First, we confirmed the successful establishment of a COL1A1-overexpressing stable cell line (COL1A1-OE cells). The plasmid vector used to overexpress COL1A1 also contained a GFP reporter gene (Fig. 5B), allowing us to visualize COL1A1-OE cells by fluorescence microscopy (Fig. 5C). While non-engineered wild-type (WT) cells showed no GFP signal, COL1A1-OE cells exhibited clear GFP expression, confirming successful plasmid integration. Elevated COL1A1 expression in COL1A1-OE cells was further validated at both the mRNA and protein levels after multiple passages (Fig. 5D and E), demonstrating that COL1A1 overexpression was stably maintained relative to WT cells.

Following the same protocols, cECM was obtained from COL1A1-OE cells (Fig. 5F). Western blot analysis further confirmed enrichment of COL1A1 in COL1A1-OE cECM relative to WT cECM when normalized to total protein (Fig. 5G). Compared with cECM derived from WT cells, COL1A1-OE cell-derived cECM contained a higher total protein yield per culture scale (Fig. 5H). Finally, CEOgel was successfully fabricated from COL1A1-enriched cECM (Fig. 5I), exhibiting stable gel formation as demonstrated by rheological properties ($G' > G''$ and $\tan\delta < 0.5$; Fig. 5J).

Altogether, we demonstrated that CEOgel composition can be customized by genetically engineering ECM-producing cells. In contrast, producing Matrigel, the most widely used animal-derived ECM hydrogel, requires induction of Engelbreth–Holm–Swarm (EHS) tumors in mice to extract basement membrane matrices rich in proteins such as laminin and type IV collagen [31,32]. Extending this strategy to other tissue-derived ECM hydrogels would demand generating transgenic animals, a process that is time-consuming, costly, and ethically restrictive. Thus, our results highlight the advantage of fabricating hydrogels directly from cell-derived ECM, where genetic engineering provides a straightforward and versatile means to tailor matrix composition.

2.5. In vitro biocompatibility and application of CEOgel

2.5.1. CEOgel demonstrates cytocompatibility without immunogenicity in vitro

To examine whether CEOgel is suitable for cell culture and regenerative studies, we evaluated its biocompatibility and performance in representative *in vitro* models. First, cell viability was assessed using two complementary culture approaches: (1) direct culture either on wells coated with a thick layer of CEOgel or within CEOgel by encapsulation,

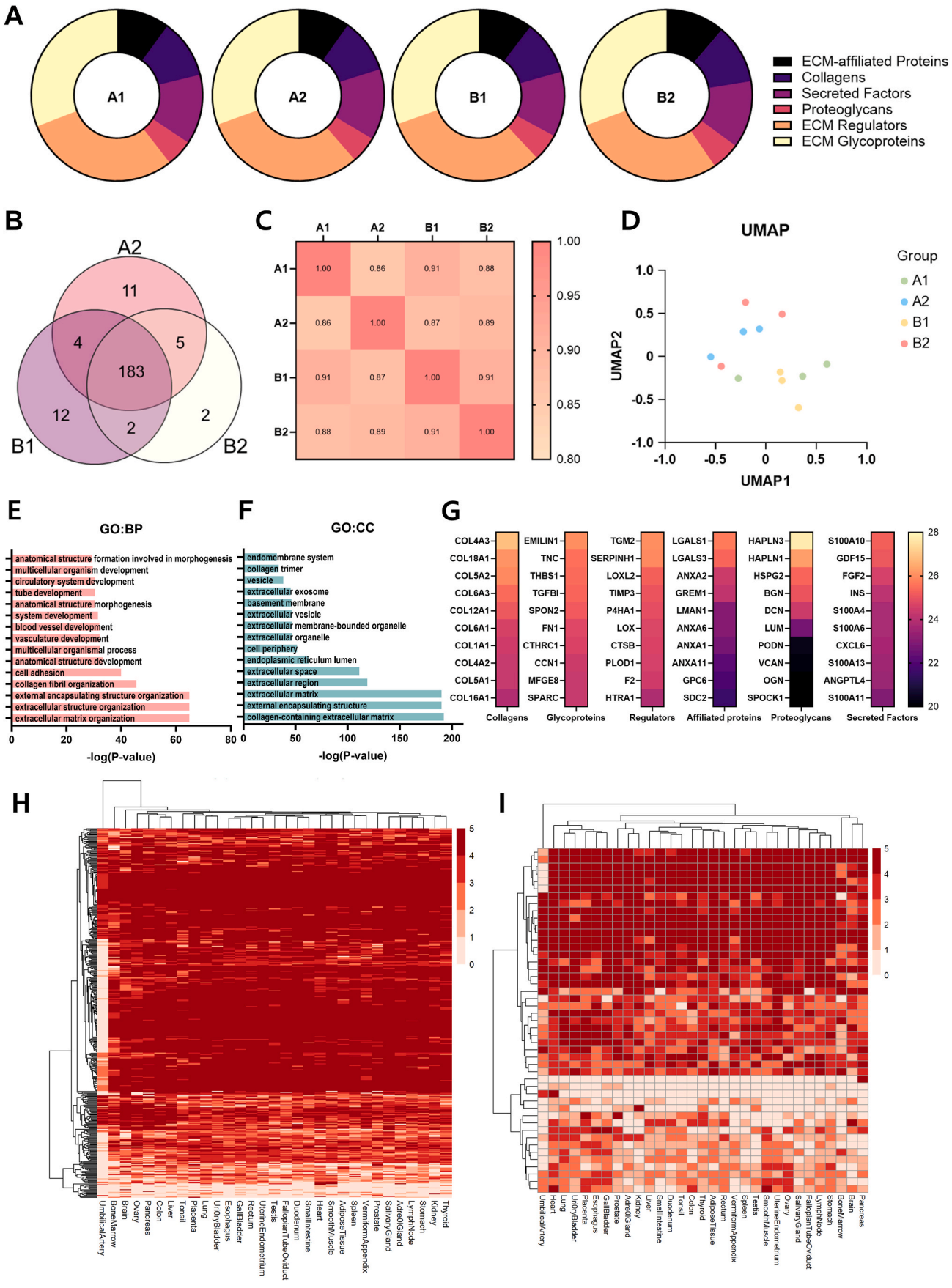

(caption on next page)

Fig. 4. Proteomic analysis of CEOgel. **(A)** The variability of total matrisome proteins among cECM samples derived from different batches of the same donor of UCMSC (Batch 1, 2) and from different donors (A, B) was compared (n = 3). **(B)** Venn diagram shows the overlap of matrisome proteins among three samples (A2, B1 and B2) **(C)** Pearson's correlation analysis was conducted to evaluate the similarity of matrisome protein profile across cECM samples from different donors or batches. Correlation coefficients (r) are indicated in each box. **(D)** UMAP was performed on samples using their matrisome protein abundance profiles to visualize clustering by donor and batch. **(E)** Gene Ontology Biological Process (GOBP) and **(F)** Gene Ontology Cellular Component (GOCC) enrichment analyses were performed for matrisome proteins in cECM. **(G)** The top 15 matrisome proteins from each matrisome category were identified and ranked. **(H)** To compare the total and **(I)** matrisome protein profiles between cECM and human tissues, hierarchical clustering analysis was performed. The top 500 total proteins and top 50 matrisome proteins from cECM were matched to tissue proteomic datasets, and their relative expression levels were visualized as heat maps. Protein expression in each tissue was categorized from 0 (low) to 5 (high). The average values were used for analyses in panels E–I.

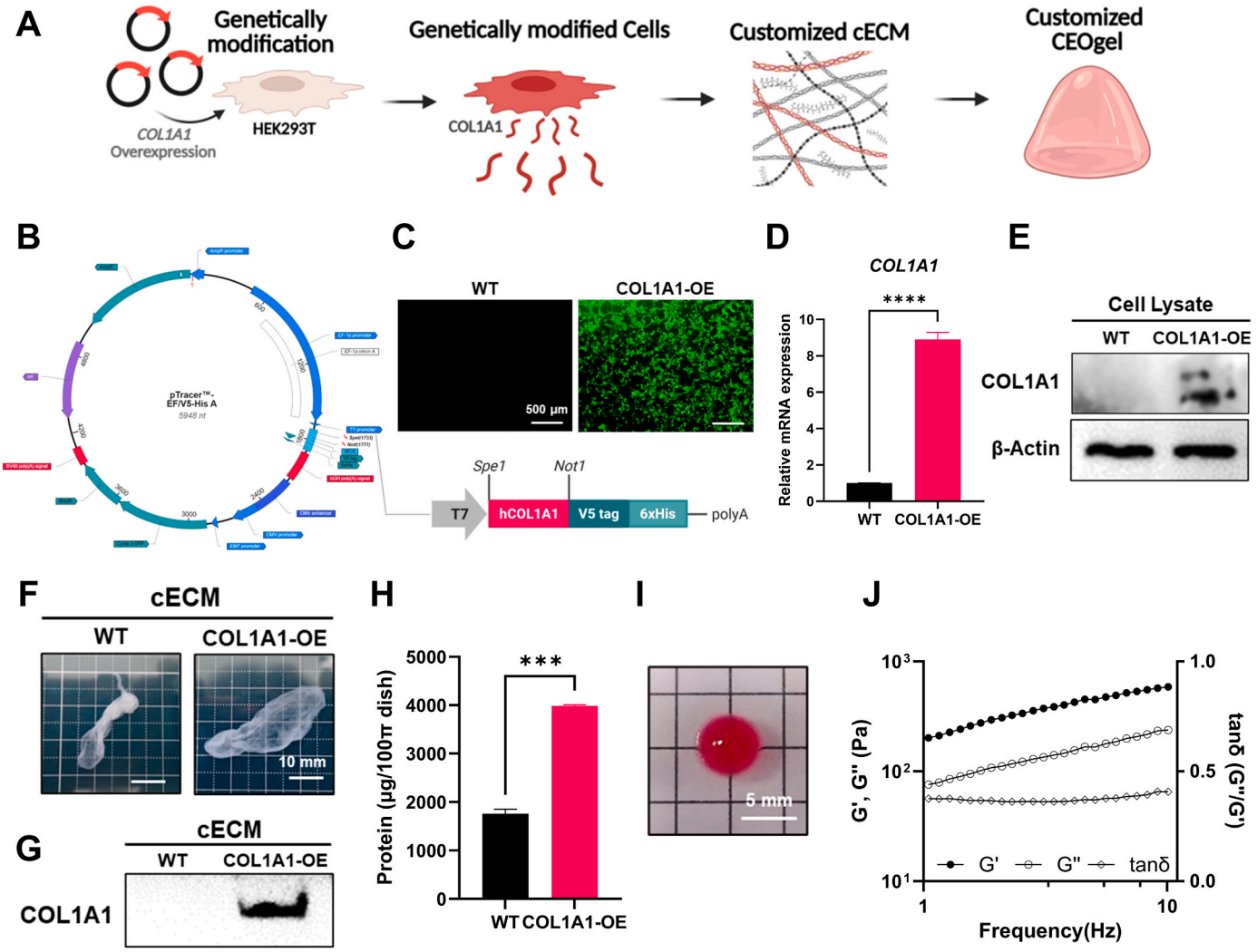

Fig. 5. Modifying components of CEOgel by genetic engineering. **(A)** The schematic shows the process used to modify CEOgel components through genetic engineering of ECM-producing cells. **(B)** The illustration depicts the plasmid vector applied in this study, indicating the target gene, promoter, and restriction enzyme sites. **(C)** Fluorescence microscopy images show GFP signals in COL1A1-OE cells, whereas wild-type (WT) cells display no fluorescence. (scale bars = 500 μm) **(D)** The mRNA expression level of COL1A1 was measured in WT and COL1A1-OE cells using qRT-PCR. **(E)** The protein level of COL1A1 was analyzed in WT and COL1A1-OE cells by western blot. **(F)** The images present decellularized cECM obtained from WT and COL1A1-OE cells. (scale bars = 10 mm) **(G)** Western blot analysis compares the relative proportion of COL1A1 in cECM derived from WT and COL1A1-OE cells, respectively. **(H)** BCA assay quantifies total protein amounts in cECM derived from WT and COL1A1-OE cells. **(I)** The image shows CEOgel fabricated from COL1A1-OE cell-derived cECM. (scale bar = 5 mm) **(J)** Rheological profiles of CEOgel derived from COL1A1-OE cells were obtained through oscillatory frequency sweep tests at 37 °C, presenting storage modulus (G′), loss modulus (G″), and tan δ. Data are shown as mean ± SD; ***$p < 0.001$, ****$p < 0.0001$, n = 3. The figure was created with BioRender.

and (2) indirect co-culture with CEOgel using a transwell system to assess non-contact effects. Three representative cell types were tested: endothelial cells (HUVEC), mesenchymal stem cells (UCMSC), and skin fibroblasts (BJ). Live/dead staining after 24 h of CEOgel-coated culture (Fig. 6A) or encapsulation (Fig. S6A) showed that the majority of cells remained viable regardless of cell type. Similarly, when they were cultured in the transwell system with CEOgel for 72 h, cell viability was not significantly different from that of non-treated control or the Matrigel- and tECMgel-treated groups. (Fig. 6B, Fig. S6B). Continuous proliferation was also observed for 7 days in all three cell types (Fig. 6C). Next, the immunogenicity of CEOgel was evaluated by co-culturing RAW 264.7 macrophages with CEOgel for 6 and 24 h. The secretion of the inflammatory cytokine, tumor necrosis factor-α (TNF-α) in CEOgel co-cultures was negligible and not statistically different from that in

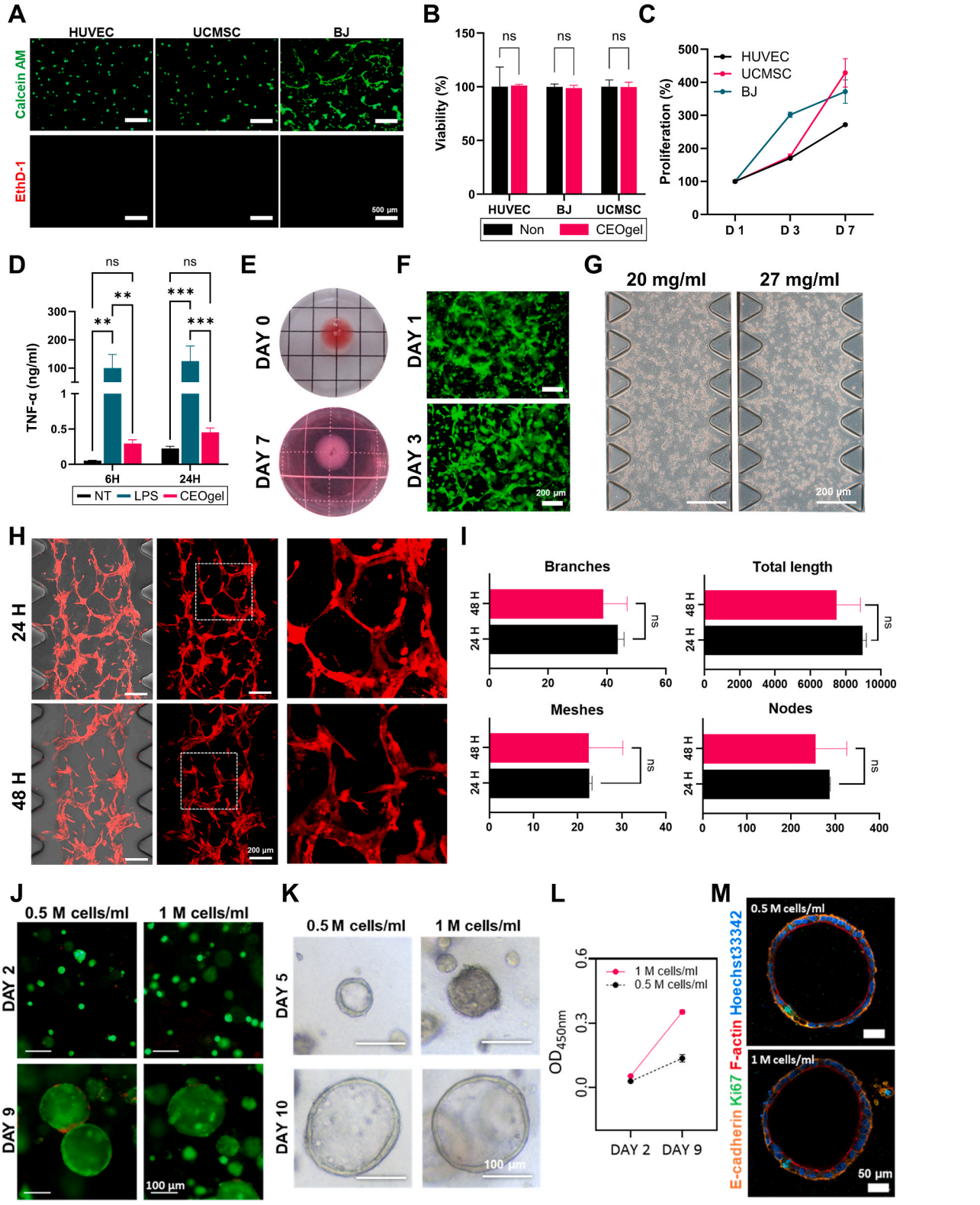

(caption on next page)

Fig. 6. Biocompatibility and application of CEOgel *in vitro*. (A) HUVEC, UCMSC, and BJ cells were cultured on CEOgel-coated plates for 24 h and stained with Calcein-AM and EthD-1 to visualize live and dead cells under a fluorescence microscope. (scale bars = 500 μm) **(B)** Cell viability was quantified by CCK-8 assay after 72 h of indirect co-culture with CEOgel in a transwell system; untreated cells served as controls. **(C)** The proliferation of HUVEC, UCMSC, and BJ cells was measured by CCK-8 assay after 7 days of incubation with CEOgel. **(D)** TNF-α secretion from RAW 264.7 macrophages was quantified after 6 h and 24 h of incubation with CEOgel; untreated and LPS-treated cells served as negative and positive controls, respectively. **(E)** Images show CEOgel before and after 7 days of incubation in cell culture medium. **(F)** Calcein-AM staining visualized tube formation of HUVECs encapsulated in CEOgel after 1 and 3 days of culture. (scale bars = 200 μm) **(G)** cENF solutions at 20 and 27 mg/mL were loaded into microfluidic devices, where *in situ* gelation formed stable CEOgels. (scale bars = 200 μm) **(H)** Confocal microscopy captured RFP-HUVEC vascular network formation within CEOgel (20 mg/mL) under flow conditions after 24 and 48 h of culture. (scale bars = 200 μm) **(I)** Quantitative analysis evaluated vascular network parameters, including the number of branch points, meshes, nodes, and total length. **(J)** Live/dead assays assessed cell viability of CRC organoids in CEOgel at day 2 and 9. (scale bars = 100 μm) **(K)** Bright field images show colorectal cancer (CRC) organoids grown in CEOgel at day 5 and 10. (scale bars = 100 μm) **(L)** WST-8 assays quantified CRC-organoid proliferation in CEOgel. Data are presented as mean ± SD; $^{**}p < 0.01$, $^{***}p < 0.001$, n. s. = not significant ($p > 0.05$); n = 3. **(M)** Immunofluorescence staining revealed expression of the proliferation marker, Ki-67 and the epithelial adhesion marker, E-cadherin in CRC organoids cultured in 33 mg/mL CEOgel. (scale bars = 50 μm).

non-treated control or the Matrigel and tECMgel-co-cultured groups, whereas LPS-treated positive control exhibited ~200-fold higher levels of TNF-α (Fig. 6D, Fig. S6C). These results indicate that CEOgel neither induces cytotoxicity, regardless of physical contact, nor provokes macrophage-mediated immune activation *in vitro*.

2.5.2. CEOgel supports diverse 3D cell culture applications

Since ECM-based matrices are widely used for 3D cell culture, we next evaluated the potential of CEOgel in representative *in vitro* models. As a first example, we tested vascular network formation with endothelial cells (ECs). Vascularization within 3D matrices has been extensively studied, as it is valuable both for generating vascular models and for enhancing other 3D culture systems by incorporating vessel-like structures that more closely replicate the tissue microenvironment [33].

After confirming that CEOgel remained stable for at least 7 days in serum-containing medium (Fig. 6E), HUVECs were encapsulated within CEOgel and cultured to induce tube formation (Fig. 6F). ECs began forming capillary-like structures within 24 h, and these networks remained stable for over 72 h before gradually degrading after 5 days of culture. In contrast, no clear network formation was observed in Matrigel or tECMgel under identical 3D encapsulation conditions, although partial elongation of HUVEC was detected in tECMgel (Fig. S7A). We then assessed CEOgel in a microfluidic chip. This "vessel-on-chip" platform is particularly relevant for endothelial studies because ECs *in vivo* are constantly exposed to shear stress [34]. EC-suspended cENF sol was loaded into the gel channel of the chip, where CEOgel was formed successfully and encapsulated ECs at concentrations ranging from 20 to 33 mg/mL (Fig. 6G). Under flow conditions, encapsulated ECs organized into capillary-like networks within 24 h (Fig. 6H), and these structures were sustained for more than 48 h without significant differences in quantitative tube-formation parameters (Fig. 6I). In contrast, ECs encapsulated in Matrigel or tECMgel did not form network structures within the microfluidic system (Fig. S7B).

Importantly, CEOgel's ability to be loaded into the chip and form a stable gel demonstrates the superiority of our cell-derived ECM hydrogel fabrication method. In previous studies, cell-derived ECM typically had to be combined with other materials such as collagen, fibrin, or chemical cross-linkers (e.g., genipin) to achieve gels with sufficient mechanical strength for chip applications [14]. In contrast, CEOgel alone maintained stable gel formation within the chip and promoted endothelial tube formation, underscoring its advantages as a versatile cell-derived ECM matrix. These results are also consistent with our proteomic analysis, which revealed enrichment of GOBP terms related to blood vessel, vasculature, and tube development (Fig. 4E).

Notably, CEOgel more effectively supported endothelial network formation under 3D culture conditions. Under 2D coating conditions, however, Matrigel supported robust capillary-like network formation within 16 h. In contrast, neither CEOgel nor tECMgel induced clear tube formation. HUVECs cultured on CEOgel exhibited slight cellular movement, whereas cells on tECMgel showed no obvious morphological changes (Fig. S7C). These results indicate that matrix performance is highly context-dependent. While Matrigel is well-suited for 2D coating-based assays, CEOgel provides a more favorable microenvironment for 3D endothelial network formation. Previous studies have shown that ECM substrates differ in their ability to support endothelial encapsulation and network formation [35–37]. In this context, our results suggest that CEOgel provides a favorable microenvironment for HUVEC encapsulation and vascular-like network formation in 3D culture, highlighting its potential as a versatile cell culture matrix.

2.5.3. CEOgel holds potential as a matrix for organoid culture

Upon the capability of CEOgel to sustain vascular-like networks in bulk gels and microfluidic systems, we next investigated its suitability for a complex 3D culture model, organoids. Colorectal cancer (CRC) organoids adapted to the ECM microenvironment provided by CEOgel, maintaining viability and proliferative activity for up to 9 days (Fig. 6J and K). Live/Dead staining demonstrated high cell viability at both day 2 and day 9 (Fig. 6J), comparable to that of organoids cultured in Matrigel (Fig. S8A). CRC organoids were successfully established at initial densities of 0.5×10^6 and 1×10^6 cells/mL, reaching approximately 100 μm in diameter by day 5 and 200 μm by day 10 (Fig. 6K). Consistent with other decellularized ECM-based biomaterials, CEOgel supported moderately slower proliferation and organoid development compared with Matrigel (Fig. S8B and C) [26,27,38], likely reflecting the differences in growth factor contents and ECM compositions between the two materials. Nevertheless, higher initial cell densities enhanced survival and promoted more robust proliferation (Fig. 6L). Immunofluorescence analysis confirmed that CRC organoids cultured in CEOgel expressed the epithelial junction marker, E-cadherin and the proliferation marker, Ki-67 after 10 days (Fig. 6M). Organoids also developed basolateral-out polarity, consistent with the morphology of tumor organoids cultured in Matrigel (Fig. S8D) and other ECM-based substrates [39]. These results indicate that CEOgel provides a permissive microenvironment for CRC organoid survival and development, highlighting its potential as a biocompatible 3D matrix for organoid culture. Optimization of cell density and culture parameters may further improve performance. Moreover, since ECM composition strongly influences organoid behavior [40], tailoring CEOgel composition —by deriving it from cell types relevant to the target organ—may further improve its compatibility with specialized organoid systems.

Together, these results demonstrate the biocompatibility and broad *in vitro* applicability of CEOgel, highlighting its promise as a matrix for 3D cell culture systems. Although the reports on cell-derived ECM remain limited, the compositional diversity of ECM across tissues suggests that different cell types could generate distinct CEOgels with tailored properties [41,42]. In principle, the choice of source cell could be aligned with the intended application—for example, skin fibroblast–derived CEOgel may provide a more relevant microenvironment for skin-related models and MSC-derived CEOgel could leverage the well-documented trophic and regenerative effects of MSCs. Compared with animal-derived ECM hydrogels, which represent bulk extracts of whole tissues, cell-type–specific CEOgels could offer microenvironments that more closely reflect tissue compartments defined by specific cell types. It is therefore valuable to profile ECMs from a variety of cell types

and assess their potential to yield CEOgels with application-specific advantages. In addition, a notable practical benefit of CEOgel is that the entire fabrication process can be carried out at the bench top, without requiring animal tissues or specialized facilities. If this practical merit is combined with knowledge of diverse CEOgels derived from different cell types, it may become possible to create customized cell-culture matrixes directly in the laboratory, optimized for the specific purpose of each study.

2.6. Biosafety of CEOgel was evaluated using a subcutaneous implantation model in vivo

Due to the ease of administration and minimal invasiveness, *in situ*–formed hydrogels have been extensively explored as biomaterials [43,44]. In particular, thermosensitive hydrogels that form gels at physiological temperature can be delivered in a sol state and subsequently undergo in-situ gelation after injection. This characteristic provides several advantages for injectable applications. Injection in the sol state minimizes shear-induced deformation that can occur when pre-formed gels are forced through a needle [45]. Moreover, *in situ* gelation allows the hydrogel to conform to irregularly shaped injection sites [46]. In addition, for drug or cell delivery applications, the thermoresponsive property facilitates homogeneous mixing of therapeutic agents or cells in the sol state prior to gelation at body temperature [47]. As such, CEOgel was evaluated in a murine subcutaneous implantation model by injection to assess its performance as a thermosensitive injectable hydrogel and to assess *in vivo* safety.

First, we tested whether cENF sol in the liquid state could be injected to form CEOgel *in situ*. As shown in Fig. 7A, a high concentration of cENF sol (67 mg/mL) did not diffuse immediately when pipetted into warm PBS. Furthermore, the sol readily passed through a 26G syringe needle and formed CEOgel at 37 °C (Fig. 7B). This was also possible even using a narrower 32G needle. These results demonstrate the excellent injectability and *in situ* gel-forming ability of CEOgel, enabled by its thermosensitive characteristics.

Then, we implanted CEOgel subcutaneously in mice to assess its behavior and safety *in vivo*. As observed *in vitro*, cENF sol was easily injected through a syringe, and gelation occurred stably at the subcutaneous injection site to form CEOgel (Fig. 7C). Non-treated (NT) mice served as controls. No abnormal skin appearance, including erythema, swelling, blistering, or ulceration, was observed around the injection sites throughout the observation period.

For further analysis, skin tissues from the injection sites were harvested at 3, 10, 20 and 30 days post-implantation. At the early time point (day 3), CEOgel was clearly visible and separated from the tissue by a cellular border zone formed by recruited host cells (Fig. 7E). As cell infiltration increased over time, the cellular border zone gradually diminished. By day 30, CEOgel was difficult to distinguish from host tissue, and more importantly there was no evidence of fibrotic encapsulation indicative of an adverse foreign-body reaction (Fig. S9).

To more precisely observe the biodegradation behavior of CEOgel, residual implanted material was specifically detected using an anti-human collagen I, as CEOgel was derived from human MSCs (Fig. 7F). At day 3, human collagen type I was clearly localized at the CEOgel implantation site and was readily distinguishable from adjacent murine tissue, confirming successful *in situ* gel formation following injection. Over time, the collagen I positive signal gradually diminished and the gel was hard to be observed at the implantation site at day 30, indicating progressive biodegradation of CEOgel. In parallel, the matrix metalloproteinases 9 (MMP9), a key enzyme involved in cellular ECM degradation, increased up to day 10 and subsequently decreased over time (Fig. 7G). This temporal pattern correlated with the reduction of residual CEOgel, suggesting that MMP-mediated proteolysis contributes to CEOgel degradation. These data indicate that CEOgel underwent progressive biodegradation while integrating with host tissue.

Next, TNF-α, a representative inflammatory cytokine, was detected throughout the implanted area, which progressively decreased and was negligible at day 30 (Fig. 7H). Additionally, immune cell ($CD11b^+$), including macrophages ($F4/80^+$), were comparably localized within the cellular border zone at day 3 and became more broadly distributed throughout in the gel by day 10 (Fig. 7I). Such acute immune cell infiltration is a natural response of biomaterials interacting with host tissues [48,49]. Importantly, when this response resolves without progressing to chronic inflammation, early immune infiltration can actively promote angiogenesis, matrix remodeling, and material biodegradation [50]. Consistently, angiogenesis which is defined as the formation of new blood vessels from pre-existing capillaries through endothelial cell (EC) sprouting followed by mural cell stabilization [51] was observed within CEOgel. At day 10, infiltrating ECs ($CD31^+$) were detected within the implanted CEOgel. By day 20, mature vessels composed of ECs ($CD31^+$) covered with mural cells ($PDGFR\beta^+$) were evident (Fig. 7J), indicating active angiogenesis and vascular maturation. These findings collectively demonstrate the bio-functionality of CEOgel *in vivo*.

To further assess the potential for chronic or systemic inflammation, TNF-α and IL-6 were measured in serum at day 30. In agreement with the histological findings, serum TNF-α levels in CEOgel-treated mice were not significantly different from those of NT controls, and IL-6 was undetectable in both groups (Fig. 7D). These results indicate that CEOgel did not provoke systemic and chronic inflammation. Furthermore, histological examination of major organs (heart, liver, spleen, lung, and kidney) revealed no detectable abnormalities in CEOgel-treated mice compared with NT controls (Fig. 7K), which confirms systemic safety.

In summary, CEOgel exhibited biocompatibility, biodegradability, and bio-functionality *in vivo*. These findings highlight the strong potential of CEOgel as a promising biomaterial platform for tissue engineering and medical applications, extending beyond *in vitro* use.

Collectively, this work introduces CEOgel as a new class of thermosensitive ECM hydrogels and establishes a benchtop fabrication method that requires neither animal tissue sources nor external cross-linkers. This approach not only broadens the utility of cECM derived from diverse cell types but also enables the development of customizable ECM hydrogels. By integrating the intrinsic advantages of cECM with the customizable and phase-transitional behavior, CEOgel represents a broadly adaptable platform for regenerative medicine, tissue engineering, and biofabrication research. Beyond the *in vitro* microfluidic applications demonstrated in this study, CEOgel may also serve as a 3D cell culture matrix for disease modeling, including cancer research [51]. Specifically, CEOgel may enables the construction of cell-specific microenvironments derived from cancer cells or cancer-associated fibroblasts and may also be explored as a matrix for hydrogel-assisted *in vivo* tumor implantation [52,53]. In addition, given that tissue-derived ECM hydrogels have already been explored as bio-inks for 3D bioprinting [54,55], CEOgel is likewise anticipated to be a promising candidate for biofabrication applications. Furthermore, its injectability and *in situ* gelation suggest potential utility as a carrier for cells, drugs, or other bioactive molecules in therapeutic settings.

Despite these promising results, several limitations should be acknowledged. In this study, UCMSC-derived CEOgel was selected for most of the analyses, although the CEOgel fabrication method was confirmed to be applicable to cECM derived from different cell types. This choice was motivated by the fact that one of the key advantages of cECM is its ability to provide access to niche-specific extracellular matrices that are difficult to isolate directly from native tissues, such as mesenchymal stem cell niches. In addition, MSC-derived ECM has been widely studied in regenerative medicine and tissue engineering [56]. Nevertheless, because cECM composition depends strongly on the originating cell type, the biochemical and physical properties of CEOgel are expected to vary accordingly. Therefore, future studies should include comprehensive characterization of CEOgels derived from multiple cell types to fully establish their cell-type–specific utility. Finally, elucidating the precise mechanisms underlying CEOgel gelation remains an important subject for future investigation. Although physical

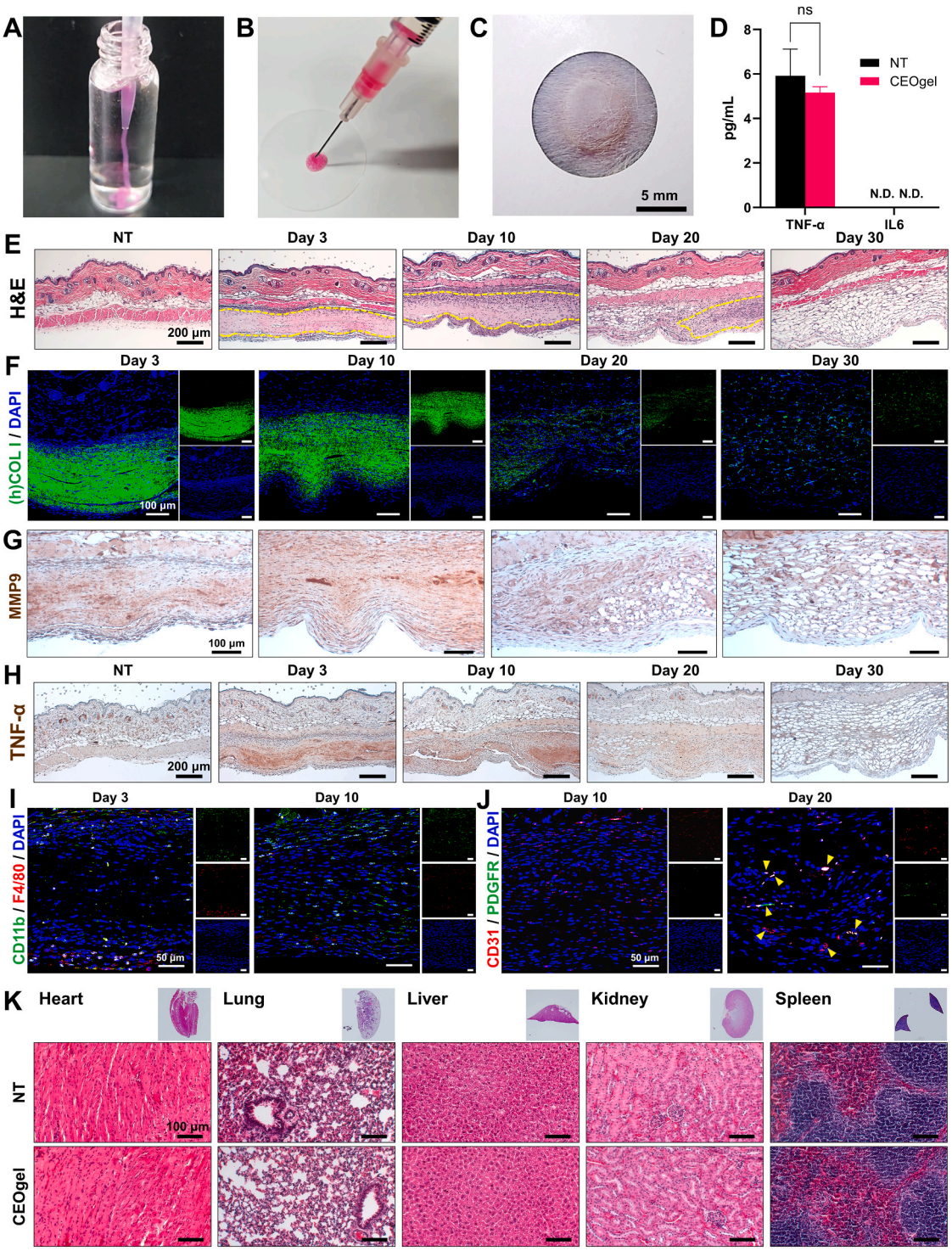

Fig. 7. Subcutaneous implantation of CEOgel and *in vivo* biosafety. **(A)** cENF solution at concentration of 67 mg/ml was extruded into warm PBS to form CEOgel. **(B)** Injectability test of 67 mg/ml cENF solution with 26G needle. **(C)** The image of mouse skin where CEOgel was subcutaneously injected. (scale bars = 5 mm) **(D)** TNF-α and IL6 level in mouse serum was measured at 30 days after subcutaneous injection of CEOgel. **(E)** The subcutaneous tissues around the CEOgel-implanted site were excised at day 3, 10, 20, and 30. And the tissue stained by H&E staining for histological analysis (scale bars: 200 μm). **(F)** Immunofluorescence (IF) staining of residual implanted CEOgel in subcutaneous tissue at the indicated time points (blue: DAPI, green: human collagen I, scale bar: 100 μm). **(G)** Immunohistochemical (IHC) staining of MMP9 in tissues surrounding the CEOgel-implantation site at different time points (scale bar: 100 μm). **(H)** Representative IHC staining of TNF-α in subcutaneous tissue surrounding the CEOgel-implanted site at different time points (scale bar: 200 μm). **(I)** Representative IF images showing immune cell infiltration at the implantation site (blue: DAPI, green: CD11b, red: F4/80, scale bar: 50 μm). **(J)** IF images showing vascularization at the CEOgel implanted site (blue: DAPI, green: PDGFRβ, red: CD31, scale bar: 50 μm). **(K)** Major organs were harvested on the 30th day after implantation of CEOgel followed by H&E staining (scale bar: 100 μm). Data are presented as mean ± SD, ns = not significant ($p > 0.05$); n = 3. (For interpretation of the references to color in this figure legend, the reader is referred to the Web version of this article.)

interactions—particularly hydrogen bonding—and the possible involvement of fiber entanglement are suggested to contribute to gel formation, additional studies are required to clarify how the individual fabrication steps collectively impart thermoreversible behavior of CEOgel.

3. Conclusion

In conclusion, this study established a novel fabrication method for a thermoreversible hydrogel, CEOgel, composed exclusively of cell-derived, decellularized ECM, without the addition of any external materials or cross-linkers. This benchtop-based platform enables the production of customized hydrogels that can be adapted to various ECM sources obtained from different cell types. The CEOgel were comprehensively analyzed—from fundamental evaluations of material properties to *in vitro* and *in vivo* assessments of biocompatibility and safety—providing a foundational understanding of this material for future applications. Proteomic analysis confirmed the negligible donor- and batch-to-batch variations of CEOgel and supported its broad applicability across different biological contexts. The promising potential of CEOgel as a 3D culture matrix was further validated through successful endothelial and organoid culture. In addition, this study demonstrated strategies to modify the properties of CEOgel, addressing the inherent limitations of natural polymer hydrogels, which are often difficult to tune. In particular, the genetic engineering approach applied to ECM-producing cells highlighted the unique advantage of using cell-derived ECM for hydrogel fabrication, demonstrating its tunability.

Overall, this study broadens the applicability of cell-derived ECM materials and expands the diversity of ECM-based hydrogels. The proposed framework contributes to the growing conceptual and technical foundation for developing and analyzing next-generation decellularized ECM hydrogels.

4. Materials and methods

4.1. Preparation of cell-derived ECM only hydrogel

4.1.1. Cell culture and decellularization

Umbilical cord mesenchymal stem cells (UCMSCs, CEFObio, Gyeonggi-do, South Korea) were seeded on tissue culture plates (TCP) at a density of 1.3×10^4 cells/cm^2 and cultured in CEFOgro Human MSC Growth Medium (CEFObio) supplemented with 10% fetal bovine serum (FBS) and 1% penicillin&streptomycin. Cells were maintained for 7 days in a humidified incubator at 37 °C with 5% CO_2 until reaching confluent.

For decellularization, cultured cells were treated with 0.25% Triton X-100 and 20 mM NH_4OH, followed by PBS rinsing. Residual nucleotides were removed by treatment with 50 U/ml DNase I (Invitrogen, Waltham, MA, USA) and 2.5 μl/ml RNase (Invitrogen) for 1 h at 37 °C. The resulting cell-derived ECM (cECM) was washed twice with PBS and stored in deionized water at −20 °C for at least 24 h prior to use. The entire process was performed in a sterile condition.

4.1.2. Fabrication of CEOgel

Frozen cECM was thawed at 37 °C and collected using a cell scraper into a conical tube. Deionized water was added, and the mixture was pulverized using an ultrasonicator (Sonic Dismembrator Model 500, Thermo Fisher Scientific, Waltham, MA, USA) to obtain a cECM suspension. The suspension was then freeze-dried for 72 h to yield cECM powder.

Pepsin (Sigma-Aldrich, St. Louis, MO, USA) was dissolved in 0.01 N HCl at a concentration of 1 mg/ml. For enzymatic digestion, 1 ml of pepsin solution was added per 10 mg of cECM powder and incubated at room temperature for 72 h with stirring. The digested cECM was neutralized to pH 7.4 ± 0.2 using 1 N NaOH and subsequently freeze-dried for 72 h. To obtain the cECM nanofiber (cENF) solution, enzyme-digested cECM powder was reconstituted in PBS at a concentration of 67 mg/ml, sonicated, and then incubated at 4 °C for at least 24 h to allow a complete dissolution. The cell-derived ECM only hydrogel (CEOgel) was formed by incubating the cENF solution at 37 °C for 30 min. Depending on the experimental purpose, the cENF solution was diluted with PBS or cell culture medium to the desired concentration.

4.2. Gelation mechanisms of CEOgel

4.2.1. Transparency

The transparency of the enzyme-digested cECM solution was evaluated before and after neutralization. Aliquots of 200 μl from each solution were loaded into a 96-well plate. Light transmittance was measured by detecting absorbance across the wavelength range of 400–800 nm using a microplate reader (Multiskan SkyHigh, Thermo Fisher Scientific, MA, USA). Deionized water was used as a control, with its % transmittance set to 100%. The transmittance of light was calculated using the following formula:

$$\% \text{ Transmittance} = 10^{2\text{-Absorbance}}$$

4.2.2. Dynamic light scattering (DLS) measurement

The particle size of cECM fibers at different stages of CEOgel fabrication was determined using dynamic light scattering (DLS). Measurements were performed on cECM suspension, enzyme-digested cECM solution, and the final cENF solution using a Zetasizer Pro ZSU3200 instrument (Malvern Instruments, Malvern, UK). Samples were analyzed at room temperature (RT) in triplicates measurement, and the data were processed using ZS XPLORER software (version 3.00).

4.2.3. Turbidity

The gelation kinetics of CEOgel were assessed by turbidimetry as previously described [57]. cENF solutions were prepared at concentrations of 67 and 33 mg/ml at 4 °C. A volume of 100 μl of each solution was dispensed into a 96-well plate, and turbidity changes were monitored using a pre-warmed microplate reader set at 37 °C. Absorbance at 405 nm was recorded every 2 min for 1.5 h (n = 3). The readings were normalized using the following equation:

$$NA = \frac{A - A_0}{A_{max} - A_0}$$

where NA is the normalized absorbance, A is the absorbance at a given time point, A_0 is the initial absorbance, and Amax is the maximum absorbance measured. Logistic regression of the time-dependent curves was used to calculate three kinetic parameters: the gelation rate (S), defined as the maximum slope of the growth phase; the half-gelation time ($t_{1/2}$), corresponding to the time required to reach 50% of maximum absorbance; and the lag time (t_{lag}), defined as the intercept of the linear growth region with the baseline (0% absorbance).

4.2.4. Tube inversion

The gelation properties of CEOgel at different concentrations were evaluated using a tube inversion test. Aliquots of 100 μl cENF solution at concentrations of 67, 33, 20, and 10 mg/ml were loaded into 1.5 ml Eppendorf tubes, inverted, and incubated at 4 °C for 1 h, after which images were taken to record the solution state. The tubes were then incubated at 37 °C for 1 h, re-inverted, and photographed to assess gel formation.

4.2.5. SDS-PAGE analysis

For SDS-PAGE analysis, the cENF solution was mixed with Laemmli sample buffer (Bio-Rad, Hercules, CA, USA) containing 10% 2-mercaptoethanol and heated at 98 °C for 5 min. After cooling, 30 μg of protein per lane was loaded onto a 4–15% gradient gel (Bio-Rad). A

standard protein marker (ExcelBand™ 3-Color Extra Range Protein Marker, SMOBIO Technology, Hsinchu City, Taiwan) was loaded in a separate lane. Electrophoresis was performed at a constant current of 15 mA. Following separation, the gel was then stained with Coomassie Brilliant Blue (Sigma-Aldrich) for 30 min and subsequently destained with a buffer consisting of water, ethanol, and acetic acid (4:5:1, v/v/v) for 3 h.

4.2.6. Molecular interaction assay

Molecular interactions of CEOgel were evaluated following the method of Zhu et al. (2022) with minor modifications. CEOgel was prepared by incubating 35 μl of cENF solution in a 12-well plate for 30 min to allow gelation. The gels were then immersed in one of three dissociation solutions: 6 M urea (Sigma-Aldrich), 0.06 M 2-mercaptoethanol (Bio-Rad), or 3 wt% sodium dodecyl sulfate (BYLABS, Gyeonggi-do, Korea), which selectively disrupt hydrogen bonds, disulfide bonds, and hydrophobic interactions, respectively. Gel size reduction was monitored by photographing at defined time points after exposure, and size changes were quantified using ImageJ software (NIH, Bethesda, MD, USA).

4.3. Characterization of CEOgel

4.3.1. Quantification of DNA, protein and glycosaminoglycan

DNA was extracted from UCMSCs and cENF sol (prepared from the same number of cells) using a DNA extraction kit (Invitrogen, Grand Island, NY, USA). The amount of extracted DNA was quantified with the Quant-iT™ PicoGreen® dsDNA assay kit (Thermo Fisher Scientific, Waltham, MA, USA) according to the manufacturer's protocol. The fluorescence signals were also detected using a microplate reader (GloMax® Discover, Promega, Madison, WI, USA). The DNA content per mg of cECM was also calculated.

Total protein and glycosaminoglycan (GAG) concentrations in the cENF sol were measured using the BCA Protein Assay Kit (Thermo Fisher Scientific) and the Glycosaminoglycans Assay Kit (Chondrex, Woodinville, WA, USA), respectively, following the manufacturers' instructions. Absorbance values were recorded with a microplate reader (Multiskan SkyHigh, Thermo Fisher Scientific), and concentrations were calculated based on standard curves.

4.3.2. Human growth factor antibody array

The growth factor composition of CEOgel was also analyzed using the Human Growth Factor Antibody Array Membrane (41 targets; ab134002, Abcam) according to the manufacturer's protocol. Briefly, membranes were first blocked and then incubated with the cENF solution overnight at 4 °C on a shaker. After washing, the membranes were sequentially incubated with biotin-conjugated anti-cytokines overnight at 4 °C with agitation and horseradish peroxidase (HRP)-conjugated streptavidin overnight at 4 °C. Following extensive washing, a chemiluminescent detection buffer was applied, and the signals were visualized using an iBright CL1500 imaging system (Invitrogen, Waltham, MA, USA). Quantitative analysis was performed using iBright Analysis Software (v4.0.1).The results were expressed as the relative ratio (%) of each target signal to the positive control. To analyze enriched GO terms associated with the 12 highly quantified growth factors, the DAVID online software was used following the developer's instructions [23,24].

4.3.3. Western blot analysis

The total protein was extracted from cells and decellularized ECM using radio-immunoprecipitation assay (RIPA) lysis buffer (Sigma-Aldrich) and 7 M urea buffer (Sigma-Aldrich), respectively, in the presence of protease inhibitors (Abcam, Cambridge, UK). Protein concentrations were determined using a BCA kit (Thermo Fisher Scientific) to ensure equal loading. Proteins were electrophoresed on SDS–polyacrylamide gels, separated, and subsequently transferred onto polyvinylidene fluoride (PVDF) membranes. The membranes were blocked with blocking buffer (BYLABS) and incubated with diluted primary antibodies at 4 °C overnight. After several washing, secondary antibodies were applied at appropriate dilutions and incubated for 1 h at room temperature. Protein bands were detected using an enhanced chemiluminescence western blotting system and visualized with an iBright 1500 imaging analyzer (Invitrogen). The following antibodies were used: Anti-Collagen I (ab138492; 1:5000) from Abcam (Cambridge, UK); Anti-Laminin beta 1 (A4373; 1:1000) from ABclonal (Woburn, MA, USA); Anti-Fibronectin (sc-9068, 1:500) from Santa Cruz (Dallas, Texas, USA); Anti-GAPDH (#97166; 1:1000), Anti-β-actin (#4967; 1:5000), horseradish peroxidase (HRP)-labeled horse anti-mouse IgG (#7076; 1:1000) and HRP-labeled goat anti-rabbit IgG (#7074; 1:1000) from Cell Signaling Technology (Danvers, MA, USA).

4.3.4. Protein visualization and immunofluorescence staining

To observe the deposition of ECM components, the CEO gel was fixed with 4% paraformaldehyde for 1 h at 37 °C and embedded in Frozen Section Compound (Leica, Wetzlar, Germany). After quick freezing, the CEO gel was cryo-sectioned at a thickness of 8 μm using a freezing microtome (Epredia™ HM 525 NX Cryostat Package, Epredia, MI, USA) and stained with Brilliant Blue R Staining Solution (B6529, Sigma-Aldrich) for 10 min at RT to visualize total proteins. In addition, the sectioned CEO gel was subjected to immunofluorescence (IF) staining to detect specific ECM components. The samples were blocked with 3% bovine serum albumin (BSA) for 1 h at RT and incubated with the primary antibodies overnight at 4 °C. After several washes, the samples were incubated with secondary antibodies for 1 h at RT and then mounted with Vectashield® mounting medium containing 4, 6-diamidino-2-phenylindole (DAPI) (H1200; Vector Lab, Burlingame, CA, USA) for counter staining. The primary and secondary antibodies used were as follows: rabbit monoclonal anti-collagen type I (ab138492, Abcam, Cambridge, UK, 1:500), rabbit polyclonal anti-laminin (L9393, Sigma-Aldrich, 1:100), mouse monoclonal anti-fibronectin (SC-8422; Santa Cruz Biotechnology, 1:200), Alexa Fluor® 488-conjugated goat anti-rabbit IgG (A-11008; Invitrogen, Waltham, MA, USA), and Alexa Fluor® 594-conjugated goat anti-mouse IgG (A-11005; Invitrogen). Fluorescence images were acquired using a FLUOVIEW™ FV4000 confocal laser scanning microscope (Olympus, Shinjuku, Japan).

4.3.5. Scanning electron microscopy (SEM)

For SEM analysis, CEOgel samples at concentration 33 and 67 mg/ml were fixed with 2.5% glutaraldehyde (Sigma-Aldrich) and 2.5% paraformaldehyde (BYLABS) in 0.1M sodium cacodylate buffer for 2h at 37 °C. After washing with 0.1M sodium cacodylate buffer, samples were dehydrated through a graded ethanol series (50, 70, 80, 90, and 100%), then completely dried using hexamethyldisilazane (HMDS, Sigma-Aldrich). The dried CEOgel samples were coated with a platinum, and their microstructures were examined uisng scanning electron microscopy (Teneo VS, FEI, Hillsboro, OR, USA).

4.3.6. Rheological characterization

The rheological properties of CEOgel were analyzed using a rheometer (MCR102; Anton Paar, Austria). A 300 μl aliquot of cENF solution at concentrations of 33 and 67 mg/ml, Matrigel (Corning, Corning, NY, USA) and liver-derived tECMgel (CellArtgen, Seoul, South Korea) was loaded onto a pre-warmed (37 °C) 25 mm parallel plate and allowed gelation for 20 min, respectively. Viscoelastic moduli were then measured at a constant strain of 1% in frequency sweep mode (1–10 Hz). Meanwhile, to assess the effect of K_2PtCl_4 on gel properties, the compound was added to the 33 mg/mL cENF solution at a final concentration of 0.5 mM prior to loading, and measurements were performed following the same protocol. Rheological measurements of hydrogels derived from COL1A1-overexpressing cell-derived ECM were carried out using the same procedure.

4.3.7. Degradation assay in vitro

Aliquots (40 μL) of cENF solution at concentrations of 33 and 67 mg/mL were placed in Eppendorf tubes and incubated at 37 °C for 1 h to induce gelation. The same volume of Matrigel and liver-derived tECMgel was used for comparison. Then, 1 ml of collagenase/dispase (0.05U/ml; Roche, Basel, Switzerland) was added to each tube for 168 h. At each time points (2, 4, 6, 8, 24, 48, 72, 96 and 168 h), 500 μl of supernatant was collected and immediately 500 μl of collagenase/dispase was immediately added to the samples to maintain a constant reaction volume. Collected samples were stored at −80 °C until analysis. Protein concentration was quantified using BCA assay kit (Thermo Fisher Scientific) according to the manufacturer's instructions. The cumulative amount of degraded protein at each time point was calculated and expressed as the percentage of the initial total protein content.

4.4. Proteomic analysis

4.4.1. Sample preparation

For lysis, cECM powder was suspended in 8 M urea (Sigma-Aldrich) prepared in 100 mM ammonium bicarbonate (ABC, Sigma-Aldrich) and sonicated for 4 min at 10 °C. The mixture was centrifuged at 16,000×*g* for 20 min at 4 °C, and the supernatant was collected. Protein concentration was determined using a BCA assay kit (Thermo Fisher Scientific). The samples were reduced with 10 mM dithiothreitol (DTT) by incubation in a thermomixer (Thermomixer 5382, Hamburg, Germany) at 37 °C for 30 min, followed by alkylation with 25 mM iodoacetamide (IAA, Sigma-Aldrich) in the dark at RT for 30 min. The urea concentration was then diluted to <1 M using 100 mM ABC, and proteins were digested with Trypsin (sequencing grade, Promega) for 16 h at 37 °C in a CO_2 incubator. The digestion was quenched with trifluoroacetic acid (TFA, Thermo Fisher Scientific) at a final concentration of 1%. Peptides were desalted using a SOLA HRP 96-well plate (Thermo Fisher Scientific), vacuum-dried with a SpeedVac (Thermo Fisher Scientific), and reconstituted in 0.1% TFA solution. The peptide concentration was measured using a Nanodrop spectrophotometer (Nano-400A, Allsheng, Hangzhou, China). All steps were conducted by the BERTIS Inc. (Gyeonggi-do, South Korea).

4.4.2. Liquid chromatography-tandem mass spectrometry (LC-MS/MS)

Protein identification by liquid chromatography–tandem mass spectrometry (LC-MS/MS) was performed using Q Exactive Orbitrap HF-X mass spectrometer (Thermo Fisher Scientific) coupled with Ultimate 3000 nanoLC system (Thermo Fisher Scientific). Samples were loaded onto a trap column (Acclaim PepMap 100, Thermo Fisher Scientific) and separated on an analytical column (PepMap RSLC C18, Thermo Fisher Scientific) at 50 °C using a 120-min gradient (5–95% solvent B; 0.1% formic acid in 80% acetonitrile with 5% DMSO) at a flow rate of 0.30 μl/min. The mass spectrometer was operated in positive-ion mode (spray voltage 2.5 kV, ion transfer tube 275 °C). Full MS1 scans were acquired at 60,000 resolution (*m/z* 350–1800), and precursor ions were fragmented by higher-energy collisional dissociation (HCD, 28% normalized collision energy). MS2 spectra were acquired at a resolution of 15,000, using an isolation window of 1.3 *m/z* and a dynamic exclusion time of 60 s. All steps were conducted by the BERTIS Inc.

4.4.3. Proteomic bioinformatics analysis

The mass spectrometry data were processed by data-dependent analysis (DDA) using SAGE software. MS/MS spectra were searched using the UniProt *Homo sapiens* reference proteome database (UP000005640). Cysteine carbamidomethylation (+57.0214 Da) was set as a fixed modification, and methionine oxidation (+15.9949 Da) as a variable modification. Enzyme specificity was defined as full tryptic digestion, allowing up to two missed cleavages, and peptide lengths of 7–50 amino acids were considered. The false discovery rate (FDR) threshold was set to 1% at the peptide, protein, and modification levels.

Label-free quantification (LFQ) values, representing normalized peptide intensities, were used for downstream analyses. Depending on the type of analysis $\log_2$-transformed data were applied. Unless otherwise specified, bioinformatic analyses were performed in R (R4.2.3). Identified proteins were annotated and classified according to the Matrisome Project to identify matrisome components in each sample. Dimensionality reduction was performed using Uniform Manifold Approximation and Projection (UMAP), and sample relationships were assessed by calculating Pearson's correlation coefficients (r). Gene ontology (GO) enrichment analysis was carried out using g:Profiler (ELIXIR, Hinxton, Cambridgeshire, UK) within R, and results were visualized accordingly. Hierarchical clustering was performed using protein expression data from native tissues reported in a recently published reference. For clustering and heatmap visualization, the top 500 most abundant proteins in the cECM and the top 50 matrisome proteins were selected.

4.5. Quantitative reverse transcription PCR (RT-qPCR)

Total RNA was extracted using an RNA extraction kit (QIAGEN, Hilden, Germany) following the manufacturer's protocol. cDNA was synthesized from the extracted RNA using SuperScript™ VILO™ Master Mix (Invitrogen, Grand Island, NY, USA). RT-qPCR was performed with TB Green® Premix Ex Taq™ (TaKaRa, Shiga, Japan) on an ABI 7500 system (Applied Biosystems, Foster City, CA, USA) using gene-specific primers. GAPDH was amplified as an endogenous control, and the relative expression levels of target genes were calculated using the $2^{-\Delta\Delta CT}$ method. Results were presented as fold changes, with the gene expression level in the control sample set to 1. All experiments were performed in triplicate. The primer sequences (5′–3′) were as follows: *GAPDH* (F: GTCAGTGGTGGACCTGACCT; R: AAAGGTGGAGGAGTGGGTGT) and *COL1A1* (F: CTGCCTGGTGAGAGAGGTCG; R: GGACCTTCAGAGCCTCGGG).

4.6. Biocompatibility test of CEOgel in vitro

4.6.1. Cell viability and proliferation

Three different cell types—UCMSCs, HUVECs (CEFObio), and BJs (ATCC, Manassas, VA, USA)—were seeded on CEOgel-coated wells at densities of 1×10^5, 1×10^6, and 1×10^5 cells/mL, respectively. After 24 h, the cells were rinsed with PBS and incubated in a working solution of 2 μM Calcein AM (Thermo Fisher Scientific) and 4 μM Ethidium Homodimer I (EthD-I, Thermo Fisher Scientific) for 30 min. The cells were then washed with PBS and imaged using a Axio Observr 3 fluorescence microscope (Carl Zeiss AG, Oberkochen, Germany).

Cytotoxicity was also assessed under non-contact conditions using a transwell system. UCMSCs, HUVECs, and BJs were seeded in 24-well plates at a density of 1×10^4 cells/well, and 20 μL of CEOgel, Matrigel or liver-derived tECMgel was loaded into the transwell inserts. Cells cultured without CEOgel served as controls. At days 1, 3, and 7, cell numbers were quantified using the Cell Counting Kit-8 (CCK-8; Dojindo, Kumamoto, Japan) according to the manufacturer's protocol. Relative viability was calculated by setting control cell viability to 100% and relative proliferation rates were calculated by normalizing cell numbers to day 1 values, which were set to 100%.

4.6.2. Immunogenicity test in vitro

RAW 264.7 cells (ATCC) were co-cultured with 20 μL of CEOgel (67 mg/mL), Matrigel or liver-derived tECMgel using a transwell system. Cells cultured without gel (NT, no treatment) and cells treated with 1 μg/mL lipopolysaccharide (LPS; Sigma-Aldrich) served as negative and positive controls, respectively. Once the conditioned media were collected at 6 h and 24 h after treatment, secreted TNF-α levels were quantified using an ELISA kit (Abclonal) according to the manufacturer's instructions.

4.7. 3D microvascular network formation in vitro

4.7.1. Encapsulation of HUVEC in CEOgel

RFP-HUVECs (Angio-Proteomie, Boston, MA, USA) or unlabeled HUVECs were suspended in the cENF solution, Matrigel or liver-derived tECMgel at a density of 2×10^6 cells/mL. Aliquots (40 μL) of the cell–matrix suspension were incubated at 37 °C in a CO_2 incubator for 1 h to induce gelation. After gelation, CEFOgro™ Human Umbilical Vein Endothelial Cell Growth Medium (EGM; CEFObio) was added. At 24 h post-encapsulation, the unlabeled HUVECs were stained with Calcein-AM (Thermo Fisher Scientific) according to the manufacturer's protocol. Tube formation was observed by Axio Observr 3 fluorescence microscopy (Carl Zeiss AG) at 24 h and 72 h after encapsulation, respectively.

4.7.2. Microvascular network formation in microfluidic chips

Microvascular networks were generated in CEOgel within microfluidic devices. RFP-HUVECs were suspended in cENF sol (20 mg/mL), Matrigel or liver-derivd tECMgel at a final density of 3×10^6 cells/mL. The cell–cENF suspension was injected into the gel channel of an idenTx 3 microfluidic chip (AIM Biotech, Nucleos, Singapore), and the chips were incubated at 37 °C for 1 h to induce gelation. Gelation was confirmed by bright-field microscopy (Axio Vert.A1, Carl Zeiss AG). EGM was then introduced into the medium channels, and different volumes were added to the four ports according to the manufacturer's instructions to prevent drying and generate medium flow. Microvascular networks were maintained within the chips at 37 °C in a CO_2 incubator with daily medium changes for 48 h, and fluorescence images were acquired at 24 h and 48 h. Network parameters were quantified using ImageJ (NIH, Bethesda, MD, USA) with the Angiogenesis Analyzer plugin.

4.8. Organoid culture

4.8.1. Human colorectal cancer (CRC) organoid culture

Human colorectal cancer (CRC) organoids used in this study were previously established and characterized [58]. Patient-derived tumor samples were collected during colorectal cancer resection surgery at Asan Medical Center (Seoul, South Korea) under Institutional Review Board approval (IRB No. 2019-0340) and with additional approval from UNIST (UNIST IRB-18-49-A). Written informed consent was obtained from all patients prior to tissue collection, and the study was conducted in accordance with the Declaration of Helsinki.

For 3D culture in CEOgel, CRC organoids that had been previously cultured in Matrigel (Corning) were collected and washed with cold DPBS using gentle pipetting. The organoids were then resuspended in TrypLE Express (Gibco, Waltham, MA, USA) and incubated at 37 °C for 10 min, followed by mechanical dissociation to obtain a single-cell suspension. The cells were washed and resuspended in cENF solution at a density of 1×10^6 cells/mL. A curing agent was added and mixed with the cell-laden cENF solution, which was immediately plated as 10–20 μL droplets and incubated upside down at 37 °C with 5% CO_2 for 10–15 min to allow gelation. After gelation, the CRC organoids were cultured with CRC organoid culture medium and maintained under standard conditions (37 °C, 5% CO_2), with medium refreshed every 3–4 days. The culture medium consisted of Advanced DMEM/F12 (Gibco) supplemented with 10% (v/v) R-spondin1 conditioned medium (Trevigen, Gaithersburg, MD, US), 5% (v/v) Fetal bovine serum (Merck, Rahway, NJ, USA), 1X B27 supplement (Gibco) 100 μg/mL Primocin (InvivoGen, San Diego, CA, USA), 5 μg/mL Plasmocin (InvivoGen), 2 mM GlutaMAX (Gibco), 10 mM HEPES (Welgene, Gyeongsangbuk-do, Korea), 10 mM Nicotinamide (Sigma-Aldrich), 1.25 mM N-acetyl-L-cysteine (Sigma-Aldrich), 100 ng/mL Noggin (Peprotech, Rocky Hill, NJ, USA), 10 μM SB202190 (Bio-gems, Westlake Village, CA), 10 nM Prostaglandin E2 (Peprotech), 50 ng/mL Animal-Free Recombinant Human EGF (Peprotech), 500 nM A83-01 (TOCRIS, Avonmouth, Bristol, UK), 10 nM Human gastrin I (Sigma-Aldrich), and 10 μM Y27632 (TOCRIS).

4.8.2. Viability of CRC organoid

For viability assessment, Live/dead staining was performed on CRC organoids embedded in CEOgel or Matrigel using calcein AM and ethidium homodimer-1 (Live/Dead Viability/Cytotoxicity Kit, Invitrogen) according to the manufacturer's instructions. Stained organoids were imaged using a fluorescence microscope (Nikon ECLIPSE Ts2; Nikon, Tokyo, Japan). The effect of 3D culture in CEOgel on cellular proliferation was assessed using the water-soluble tetrazolium salt WST-8 (Quanti-Max™ WST-8 Cell Viability Assay Kit, Biomax, Gyeonggi-do, Korea). CRC organoids encapsulated in CEOgel or Matrigel were incubated with 10% WST-8 reagent for 2 h at each predetermined time point. Absorbance was measured at 450 nm using a microplate reader (BioTek, Winooski, VT, USA).

4.8.3. Immunofluorescence staining of CRC organoid

Organoids were fixed with 4% paraformaldehyde and permeabilized with 0.2% Triton X-100 (LPS Solution, South Korea) in DPBS. To reduce nonspecific antibody binding and enhance penetration, they were incubated with 3% BSA (Sigma-Aldrich, USA) in DPBS containing 0.02% Triton X-100 for 1 h at room temperature. Organoids were then incubated with primary antibodies (E-cadherin, Proteintech; Ki67, Santa Cruz) at 4 °C for 24 h. After 2–3 washes with DPBS, organoids were incubated with secondary antibodies conjugated to Alexa Fluor 488 or 555 (Invitrogen). F-actin was visualized using Alexa Fluor 647-conjugated phalloidin (Invitrogen), and nuclei were stained with Hoechst 33342 (Invitrogen). Confocal images were acquired using a Zeiss LSM 980 confocal laser scanning microscope and subsequently analyzed with Zeiss Zen Blue software and ImageJ v1.54.

4.9. Biosafety of CEOgel in vivo

4.9.1. Injectability test

The cENF sol containing phenol red was pipetted into a glass vial filled with warm deionized water to assess injectability. The injectability of CEOgel was further evaluated using a syringe fitted with a 26G needle (Koreavaccine, Ansan-si, Gyeonggi-do, South Korea). All procedures were recorded with a digital camera, and representative images are presented in this study.

4.9.2. Subcutaneous injection of CEOgel in the mouse

The *in vivo* safety of the CEOgel was evaluated through murine subcutaneous transplantation by injection. The male BALB/c mice (6-week-old) were purchased from Orient Bio (Gapyeong, South Korea). Prior to injection, the mice were anesthetized by inhalation of isoflurane in oxygen, and the dorsal hair was shaved using clippers. After sterilization of the dorsal skin, 100 μL of CEOgel (50 μL per injection, 2 injections per mouse, $n=3$ per time points) was injected using a BD Ultra-Fine™ II Insulin Syringe (31G, Becton, Dickinson and Company, NJ, USA) and subsequently gelled *in situ* at body temperature within 30 min. On day 3, 10, 20, and 30 post-injection, the mice were euthanized using CO_2 inhalation, followed by excision of the skin tissue containing residual gels. On day 30, five major organs (heart, lung, liver, kidney, spleen) were harvested to assess organ toxicity, and blood samples were collected by cardiac puncture to evaluate immunogenicity. As a negative control, the non-treated mice (NT, $n=3$) were randomly selected at day 0 and subjected to sample harvest at day 30. All animal experiments were conducted under the compliance with the National Research Council's Guide for the Care and Use of Laboratory Animals (8th edition, NIH Publication, 2011). This study protocol was approved by the Korea Institute of Science and Technology Animal Care and Use Committee (KIST-IACUC-2022-05-083).

4.9.3. Histological and immunohistochemical analysis

Tissue samples were fixed in 10% formalin, embedded in paraffin (FFPE), and sectioned at a thickness of 5 μm using a rotary microtome (Epredia™ HM 325 Microtome, Epredia). Sections were deparaffinized with xylene and rehydrated through a graded series of alcohol solutions. Hematoxylin and eosin (H&E) was performed to observe local (subcutaneous) or organ response after CEOgel injection. Additionally, immunohistochemical (IHC) staining was carried out to examine the distribution of specific factor. After deparaffinized and rehydrated, antigen retrieval was performed using antigen unmasking solution (H-3300, Vector Lab), and endogenous peroxidase activity was blocked with BLOXALL Blocking Solution (SP-6000, Vector Lab) for 10 min. Following several washes with tris-buffered saline (TBS), tissues were blocked with 2.5% normal horse serum (NHS), incubated with primary antibody (rabbit monoclonal anti-TNF alpha, ab183218, Abcam, 1:500) and matrix metallopeptidase 9 (MMP9) (Mouse monoclonal anti-MMP9, MA5-15886, Invitrogen, 1:200) in 1% NHS for 30 min, treated with biotinylated universal antibody (BUA, anti-mouse/rabbit IgG) for 30 min, and then incubated with avidin-biotin complex (ABC) reagent for 30 min, which are contained in VETASTAIN Elite ABC-HRP kit (PK-7200, Vector Lab). The color development was achieved using ImmPACT® DAB Substrate Kit (SK-4105, horseradish peroxidase (HRP), Vector Lab), followed by counterstaining with Hematoxylin QS (H-3404) for 30 s. After being rinsed with DW, stained tissues were mounted with VectaMount QA Mounting Medium (H-5501, Vector Lab) and covered with a coverslip. High resolution images were randomly acquired using an inverted microscope (Axio Vert.A1; Carl Zeiss, Oberkochen, Germany)

To further analyze specific cells and implanted CEOgel, IF staining was performed using selected protein markers. FFPE tissue sections were deparaffinized and rehydrated, followed by antigen retrieval via microwave heating in citrate buffer (pH 6). Sections were blocked with 1% BSA to prevent non-specific binding. Primary antibodies were applied overnight at 4 °C. After thorough washing with PBS, sections were incubated with appropriate fluorophore-conjugated secondary antibodies for 1 h at RT in the dark. Nuclei were counterstained with NucBlue™ Fixed Cell ReadyProbes™ Reagent-DAPI (R37606, Invtirogen), and sections were mounted using VECTASHIELD® Antifade Mounting Medium (H-1000; Vector Lab). The primary antibodies used were as follows: monoclonal anti-CD11b (M1/70)-conjugated 488 (53-0112-82, Invitrogen, 1:200) for immune cells; rat monoclonal anti-F4/80 (ab16911, Abcam, 1:200) for macrophages; rabbit polyclonal anti-CD31 (ab28364, Abcam, 1:100) for endothelial cells; mouse monoclonal anti-PDGFRβ (ab69506, Abcam, 1:100) for mural cells; and rabbit monoclonal anti-Collagen I (reactive to human, ab138492, Abcam, 1:500) to detect residual CEOgel. Secondary antibodies included: Anti-rat Alexa Fluor 594 Goat antibody (ab150160, Abcam, 1:200), Anti-rabbit Alexa Fluor 594 Donkey (A21207, Invitrogen, 1:200), Anti-mouse Alexa Fluor 488 Donkey (A11001, Invitrogen, 1:200), and Anti-rabbit Alexa Fluor 488 Goat antibody (A11008, Invitrogen, 1:200). Fluorescence images were acquired using a FLUOVIEW™ FV4000 confocal laser scanning microscope (Olympus, Shinjuku, Japan).

4.9.4. Immunogenicity test in vivo

At 30 days after CEOgel injection, whole blood was collected from euthanized animals by cardiac puncture. To obtain serum, the blood samples were incubated at RT for 30 min and centrifuged at 1500×*g* for 10 min at 4 °C. The supernatant was transferred and subjected to a second centrifugation under the same conditions, after which the serum was collected and stored at −80 °C. Both TNF-α and IL-6 in the serum were quantified using ELISA kits (Abclonal) according to the manufacturer's instructions. Serum from untreated mice served as a normal control.

4.10. Statistical analysis

Statistical analyses and graphical representations were mostly performed using GraphPad Prism 10 (GraphPad, MA, USA). Comparisons between two dependent groups were conducted using the Student's t-test. For multiple group comparisons, one-way ANOVA followed by Tukey's post hoc test was applied. Data are presented as mean ± standard deviation (S.D.). A p-value <0.05 was considered statistically significant. Statistical significance was indicated as $^{**}p < 0.01$, $^{***}p < 0.001$, and $^{****}p < 0.0001$.

Funding source

This research was supported by the Korean Fund for Regenerative Medicine (KFRM)grant (25A0206L1) funded by the Ministry of Science and ICT, Republic of Korea. This research was also funded by the Ministry of Science and ICT, Republic of Korea (RS-2024-00449435).

CRediT authorship contribution statement

Byoungha An: Conceptualization, Formal analysis, Investigation, Methodology, Software, Visualization, Writing – original draft, Writing – review & editing. **Jae Won Kwon:** Investigation, Methodology, Software, Visualization. **Heejeong Yoon:** Investigation, Methodology, Visualization. **Tae-Eun Park:** Investigation, Methodology, Visualization. **Seung Won Yang:** Investigation, Methodology, Software. **Kwideok Park:** Funding acquisition, Project administration, Supervision, Writing – review & editing.

Declaration of competing interest

The authors declare that they have no known competing financial interests or personal relationships that could have appeared to influence the work reported in this paper.

Acknowledgements

The author would like to thank Dr. Soo-Hong Lee for providing cells. All schematic illustrations were created using BioRender.

Appendix A. Supplementary data

Supplementary data to this article can be found online at https://doi.org/10.1016/j.mtbio.2026.103040.

Data availability

Data will be made available on request.

References

[1] C. Frantz, K.M. Stewart, V.M. Weaver, The extracellular matrix at a glance, J. Cell Sci. 123 (24) (2010) 4195.
[2] Z. Chen, C. Du, S. Liu, J. Liu, Y. Yang, L. Dong, W. Zhao, W. Huang, Y. Lei, Progress in biomaterials inspired by the extracellular matrix, Giant 19 (2024) 100323.
[3] G.S. Hussey, J.L. Dziki, S.F. Badylak, Extracellular matrix-based materials for regenerative medicine, Nat. Rev. Mater. 3 (7) (2018) 159–173.
[4] J.M. Aamodt, D.W. Grainger, Extracellular matrix-based biomaterial scaffolds and the host response, Biomaterials 86 (2016) 68–82.
[5] A.H. Morris, H. Lee, H. Xing, D.K. Stamer, M. Tan, T.R. Kyriakides, Tunable hydrogels derived from genetically engineered extracellular matrix accelerate diabetic wound healing, ACS applied materials & interfaces 10 (49) (2018) 41892–41901.
[6] J.-E.W. Ahlfors, K.L. Billiar, Biomechanical and biochemical characteristics of a human fibroblast-produced and remodeled matrix, Biomaterials 28 (13) (2007) 2183–2191.
[7] S. Zhang, Y. Guo, Y. Lu, F. Liu, B.C. Heng, X. Deng, The considerations on selecting the appropriate decellularized ECM for specific regeneration demands, Mater. Today Bio 29 (2024) 101301.

[8] A.A. Golebiowska, J.T. Intravaia, V.M. Sathe, S.G. Kumbar, S.P. Nukavarapu, Decellularized extracellular matrix biomaterials for regenerative therapies: advances, challenges and clinical prospects, Bioact. Mater. 32 (2024) 98–123.
[9] J.W. Kwon, C. Savitri, B. An, S.W. Yang, K. Park, Mesenchymal stem cell-derived secretomes-enriched alginate/extracellular matrix hydrogel patch accelerates skin wound healing, Biomater. Res. 27 (1) (2023) 107.
[10] G.H. Chen, K.-C. Sia, S.-W. Liu, Y.-C. Kao, P.-C. Yang, C.-H. Ho, S.-C. Huang, P.-Y. Lee, M.-Z. Liang, L. Chen, Implantation of MSC spheroid-derived 3D decellularized ECM enriched with the MSC secretome ameliorates traumatic brain injury and promotes brain repair, Biomaterials 315 (2025) 122941.
[11] I.G. Kim, M.P. Hwang, J.S. Park, S.H. Kim, J.H. Kim, H.J. Kang, R. Subbiah, U. H. Ko, J.H. Shin, C.H. Kim, D. Choi, K. Park, Stretchable ECM patch enhances stem cell delivery for Post-MI cardiovascular repair, Adv Healthc Mater 8 (17) (2019) e1900593.
[12] C. Savitri, S.S. Ha, J.W. Kwon, S.H. Kim, Y.M. Kim, H.M. Park, H. Kwon, M.J. Ji, K. Park, Human fibroblast-derived matrix hydrogel accelerates regenerative wound remodeling through the interactions with macrophages, Adv. Sci. (Weinh.) 11 (18) (2024) e2305852.
[13] V.H.G. Phan, M. Murugesan, P. Manivasagan, T.L. Nguyen, T.H. Phan, C.H. Luu, D. K. Ho, Y. Li, J. Kim, D.S. Lee, T. Thambi, Injectable hydrogel based on protein-polyester microporous network as an implantable niche for active cell recruitment, Pharmaceutics 14 (4) (2022).
[14] E.L. Doherty, G. Krohn, E.C. Warren, A. Patton, C.P. Whitworth, M. Rathod, A. Biehl, W.Y. Aw, D.O. Freytes, W.J. Polacheck, Human cell-derived matrix composite hydrogels with diverse composition for use in vasculature-on-chip models, Adv. Healthcare Mater. 13 (19) (2024) 2400192.
[15] L.T. Saldin, M.C. Cramer, S.S. Velankar, L.J. White, S.F. Badylak, Extracellular matrix hydrogels from decellularized tissues: structure and function, Acta Biomater. 49 (2017) 1–15.
[16] T. Suezawa, N. Sasaki, Y. Yukawa, N. Assan, Y. Uetake, K. Onuma, R. Kamada, D. Tomioka, H. Sakurai, R. Katayama, Ultra-rapid and specific gelation of collagen molecules for transparent and tough gels by transition metal complexation, Adv. Sci. 10 (30) (2023) 2302637.
[17] Y.-H. Kim, G. Cidonio, J.M. Kanczler, R.O. Oreffo, J.I. Dawson, Human bone tissue-derived ECM hydrogels: controlling physicochemical, biochemical, and biological properties through processing parameters, Bioact. Mater. 43 (2025) 114–128.
[18] S.D. Sackett, D.M. Tremmel, F. Ma, A.K. Feeney, R.M. Maguire, M.E. Brown, Y. Zhou, X. Li, C. O'Brien, L. Li, Extracellular matrix scaffold and hydrogel derived from decellularized and delipidized human pancreas, Sci. Rep. 8 (1) (2018) 10452.
[19] A. Viswanath, J. Vanacker, L. Germain, J.G. Leprince, A. Diogenes, K. M. Shakesheff, L.J. White, A. des Rieux, Extracellular matrix-derived hydrogels for dental stem cell delivery, J. Biomed. Mater. Res. 105 (1) (2017) 319–328.
[20] M. Du, E. Zhao, J. Li, Y. Yao, Y. Wang, J. Chen, C. Qu, Rapid sol-gel reversible thermosensitive collagen for 3D cell culture, Colloids Surf. A Physicochem. Eng. Asp. 681 (2024) 132813.
[21] P. Zhu, W. Huang, L. Chen, Develop and characterize thermally reversible transparent gels from pea protein isolate and study the gel formation mechanisms, Food Hydrocoll. 125 (2022) 107373.
[22] P.M. Crapo, T.W. Gilbert, S.F. Badylak, An overview of tissue and whole organ decellularization processes, Biomaterials 32 (12) (2011) 3233–3243.
[23] D.W. Huang, B.T. Sherman, R.A. Lempicki, Systematic and integrative analysis of large gene lists using DAVID bioinformatics resources, Nat. Protoc. 4 (1) (2009) 44–57.
[24] B.T. Sherman, M. Hao, J. Qiu, X. Jiao, M.W. Baseler, H.C. Lane, T. Imamichi, W. Chang, DAVID: a web server for functional enrichment analysis and functional annotation of gene lists (2021 update), Nucleic Acids Res. 50 (W1) (2022) W216–W221.
[25] X. Shao, C.D. Gomez, N. Kapoor, J.M. Considine, C. Grams, Y. Gao, A. Naba, MatrisomeDB 2.0: 2023 updates to the ECM-protein knowledge database, Nucleic Acids Res. 51 (D1) (2023) D1519–D1530.
[26] G.G. Giobbe, C. Crowley, C. Luni, S. Campinoti, M. Khedr, K. Kretzschmar, M.M. De Santis, E. Zambaiti, F. Michielin, L. Meran, Extracellular matrix hydrogel derived from decellularized tissues enables endodermal organoid culture, Nat. Commun. 10 (1) (2019) 5658.
[27] S. Kim, S. Min, Y.S. Choi, S.-H. Jo, J.H. Jung, K. Han, J. Kim, S. An, Y.W. Ji, Y.-G. Kim, Tissue extracellular matrix hydrogels as alternatives to Matrigel for culturing gastrointestinal organoids, Nat. Commun. 13 (1) (2022) 1692.
[28] A. Prakash, D. García-Seisdedos, S. Wang, D.J. Kundu, A. Collins, N. George, P. Moreno, I. Papatheodorou, A.R. Jones, J.A. Vizcaíno, Integrated view of baseline protein expression in human tissues, J. Proteome Res. 22 (3) (2022) 729–742.
[29] M. Uhlén, L. Fagerberg, B.M. Hallström, C. Lindskog, P. Oksvold, A. Mardinoglu, Å. Sivertsson, C. Kampf, E. Sjöstedt, A. Asplund, Tissue-based map of the human proteome, Science 347 (6220) (2015) 1260419.
[30] Z. Jiang, N. Li, D. Zhu, L. Ren, Q. Shao, K. Yu, G. Yang, Genetically modified cell sheets in regenerative medicine and tissue engineering, Biomaterials 275 (2021) 120908.
[31] M.C. Kibbey, Maintenance of the EHS sarcoma and Matrigel preparation, J. Tissue Cult. Methods 16 (3) (1994) 227–230.
[32] A. Passaniti, H.K. Kleinman, G.R. Martin, Matrigel: history/background, uses, and future applications, Journal of cell communication and signaling 16 (4) (2022) 621–626.
[33] S.G. Anthon, K.P. Valente, Vascularization strategies in 3D cell culture models: from scaffold-free models to 3D bioprinting, Int. J. Mol. Sci. 23 (23) (2022) 14582.
[34] H. Yang, T. Chen, Y. Hu, F. Niu, X. Zheng, H. Sun, L. Cheng, L. Sun, A microfluidic platform integrating dynamic cell culture and dielectrophoretic manipulation for in situ assessment of endothelial cell mechanics, Lab Chip 23 (16) (2023) 3581–3592.
[35] X. Feng, M.G. Tonnesen, S.A. Mousa, R.A. Clark, Fibrin and collagen differentially but synergistically regulate sprout angiogenesis of human dermal microvascular endothelial cells in 3-dimensional matrix, International journal of cell biology 2013 (1) (2013) 231279.
[36] R.R. Rao, A.W. Peterson, J. Ceccarelli, A.J. Putnam, J.P. Stegemann, Matrix composition regulates three-dimensional network formation by endothelial cells and mesenchymal stem cells in collagen/fibrin materials, Angiogenesis 15 (2) (2012) 253–264.
[37] R.E. Fitzsimmons, R.G. Ireland, A. Zhong, A. Soos, C.A. Simmons, Assessment of fibrin-collagen co-gels for generating microvessels ex vivo using endothelial cell-lined microfluidics and multipotent stromal cell (MSC)-induced capillary morphogenesis, Biomed. Mater. 16 (3) (2021) 035005.
[38] H. Song, H. Jiang, W. Hu, Y. Hai, Y. Cai, H. Li, Y. Liao, Y. Huang, X. Lv, Y. Zhang, J. Zhang, Y. Huang, X. Liang, H. Huang, X. Lin, Y. Wang, X. Yi, Cervical extracellular matrix hydrogel optimizes tumor heterogeneity of cervical squamous cell carcinoma organoids, Sci. Adv. 10 (20) (2024) eadl3511.
[39] J.Y. Co, M. Margalef-Catala, D.M. Monack, M.R. Amieva, Controlling the polarity of human gastrointestinal organoids to investigate epithelial biology and infectious diseases, Nat. Protoc. 16 (11) (2021) 5171–5192.
[40] L. Zhu, J. Yuhan, H. Yu, B. Zhang, K. Huang, L. Zhu, Decellularized extracellular matrix for remodeling bioengineering organoid's microenvironment, Small 19 (25) (2023) e2207752.
[41] Z. Li, D.M. Tremmel, F. Ma, Q. Yu, M. Ma, D.G. Delafield, Y. Shi, B. Wang, S. A. Mitchell, A.K. Feeney, V.S. Jain, S.D. Sackett, J.S. Odorico, L. Li, Proteome-wide and matrisome-specific alterations during human pancreas development and maturation, Nat. Commun. 12 (1) (2021) 1020.
[42] M.C. McCabe, A.J. Saviola, K.C. Hansen, Mass spectrometry-based Atlas of extracellular matrix proteins across 25 mouse organs, J. Proteome Res. 22 (3) (2023) 790–801.
[43] X. Li, D. Zhao, K.J. Shea, X. Li, X. Lu, In situ formed thermogelable hydrogel photonic crystals assembled by thermosensitive IPNs, Mater. Horiz. 8 (3) (2021) 932–938.
[44] A.A. Thorpe, C. Freeman, P. Farthing, J. Callaghan, P.V. Hatton, I.M. Brook, C. Sammon, C.L. Le Maitre, In vivo safety and efficacy testing of a thermally triggered injectable hydrogel scaffold for bone regeneration and augmentation in a rat model, Oncotarget 9 (26) (2018) 18277–18295.
[45] M. Jamadi Khiabani, S. Soroushzadeh, A. Talebi, A. Samanta, Shear-induced cycloreversion leading to shear-thinning and autonomous self-healing in an injectable, shape-holding collagen hydrogel, ACS Appl. Mater. Interfaces 16 (41) (2024) 55056–55070.
[46] R. Dimatteo, N.J. Darling, T. Segura, Forming injectable hydrogels for drug delivery and wound repair, Adv Drug Deliver Rev 127 (2018) 167–184.
[47] H.Z. Deng, A.J. Dong, J.B. Song, X.Y. Chen, Injectable thermosensitive hydrogel systems based on functional PEG/PCL block polymer for local drug delivery, J. Contr. Release 297 (2019) 60–70.
[48] A. Carnicer-Lombarte, S.T. Chen, G.G. Malliaras, D.G. Barone, Foreign body reaction to implanted biomaterials and its impact in nerve neuroprosthetics, Front. Bioeng. Biotechnol. 9 (2021) 622524.
[49] N.M.M. Peltokallio, R. Ajdary, G. Reyes, E. Kankuri, J.J.T. Junnila, S. Kuure, A. S. Meller, J. Kuula, E. Raussi-Lehto, H. Sariola, O.M. Laitinen-Vapaavuori, O. J. Rojas, Comparative in vivo biocompatibility of cellulose-derived and synthetic meshes in subcutaneous transplantation models, Biomacromolecules 25 (11) (2024) 7298–7310.
[50] L. Zhang, U. D'Amora, A. Ronca, Y. Li, X. Mo, F. Zhou, M. Yuan, L. Ambrosio, J. Wu, M.G. Raucci, In vitro and in vivo biocompatibility and inflammation response of methacrylated and maleated hyaluronic acid for wound healing, RSC Adv. 10 (53) (2020) 32183–32192.
[51] Z. Chen, J. Wang, R.K. Kankala, M. Jiang, L. Long, W. Li, L. Zou, A. Chen, Y. Liu, Decellularized extracellular matrix-based disease models for drug screening, Mater. Today Bio 29 (2024) 101280.
[52] G. Benton, I. Arnaoutova, J. George, H.K. Kleinman, J. Koblinski, Matrigel: from discovery and ECM mimicry to assays and models for cancer research, Adv Drug Deliver Rev 79 (2014) 3–18.
[53] J.X. Huang, B. Sun, W. McGahan, D.J. Cavallucci, T. O'Rourke, C. Liu, Y. He, J. D. Hooper, Indocyanine green-labeled antibodies cotargeting CDCP1 and Mesothelin for fluorescence-guided imaging of pancreatic cancer, Mol. Pharm. (2026).
[54] B.S. Kim, M. Ahn, W.-W. Cho, G. Gao, J. Jang, D.-W. Cho, Engineering of diseased human skin equivalent using 3D cell printing for representing pathophysiological hallmarks of type 2 diabetes in vitro, Biomaterials 272 (2021) 120776.
[55] M. Kim, D. Kang, H. Han, J. Jang, Light-activated decellularized extracellular matrix-based bioinks for enhanced mechanical integrity, Mater. Today Bio (2025) 101859.
[56] X. Zhang, Y. Liu, K.L. Clark, A.-M. Padget, P.G. Alexander, J. Dai, W. Zhu, H. Lin, Mesenchymal stem cell-derived extracellular matrix (mECM): a bioactive and

versatile scaffold for musculoskeletal tissue engineering, Biomed. Mater. 16 (1) (2020) 012002.

[57] D.O. Freytes, J. Martin, S.S. Velankar, A.S. Lee, S.F. Badylak, Preparation and rheological characterization of a gel form of the porcine urinary bladder matrix, Biomaterials 29 (11) (2008) 1630–1637.

[58] S. Lee, K. Kim, H.J. Jeong, S. Choi, H. Cheng, D. Kim, S. Heo, J. Mun, M. Kim, E. Lee, Y.J. Choi, S.G. Lee, E.A. Lee, Y. Jang, K. Lim, H.S. Kim, E. Jeong, S. J. Myung, D.B. Jung, C.S. Yu, I.H. Song, M.R. Corces, J.H. Kang, K. Myung, T. Kwon, T.E. Park, J. Joo, S.W. Cho, Combining multiplexed CRISPR/Cas9-Nickase and PARP inhibitors efficiently and precisely targets cancer cells, Cancer Res. 85 (15) (2025) 2890–2904.